Journal of Computational Physics 272 (2014) 23–45

Contents lists available at ScienceDirect

Journal of Computational Physics

www.elsevier.com/locate/jcp

A fast finite volume solver for multi-layered shallow water flows with mass exchange

Emmanuel Audusse [a,b], Fayssal Benkhaldoun [b,*], Saida Sari [b], Mohammed Seaid [c], Pablo Tassi [d]

[a] INRIA Paris-Rocquencourt, Domaine de Voluceau, 78153 le Chesnay, France
[b] LAGA, Université Paris 13, Sorbonne Paris Cité, 99 Av J.B. Clement, 93430 Villetaneuse, France
[c] School of Engineering and Computing Sciences, University of Durham, UK
[d] Laboratoire National d'Hydraulique et Environnement, 78401 Chatou Cedex, France

ARTICLE INFO

Article history:
Received 12 November 2012
Received in revised form 7 April 2014
Accepted 9 April 2014
Available online 16 April 2014

Keywords:
Multi-layer shallow water equations
Hydrostatic flows
Finite volume method
Method of characteristics
Mass exchange
Wind-driven flows

ABSTRACT

A fast finite volume solver for hydrostatic multi-layered shallow water flows with mass exchange is investigated. In contrast to many models for multi-layered hydrostatic shallow water flows where the immiscible suppression is assumed, the present model allows for mass exchange between the layers. The multi-layered shallow water equations form a system of conservation laws with source terms for which the computation of the eigenvalues is not trivial. For most practical applications, complex eigenvalues may arise in the system and the multi-layered shallow water equations are not hyperbolic anymore. This property makes the application of conventional finite volume methods difficult or even impossible for those methods that require in their formulation the explicit computation of the eigenvalues. In the current study, we propose a finite volume method that avoids the solution of Riemann problems. At each time step, the method consists of two stages to update the new solution. In the first stage, the multi-layered shallow water equations are rewritten in a non-conservative form and the intermediate solutions are calculated using the method of characteristics. In the second stage, the numerical fluxes are reconstructed from the intermediate solutions in the first stage and used in the conservative form of the multi-layered shallow water equations. The proposed method is simple to implement, satisfies the conservation property and is suitable for multi-layered shallow water equations on non-flat topography. The proposed finite volume solver is verified against several benchmark tests and it shows good agreement with analytical solutions of the incompressible hydrostatic Navier–Stokes equations. The method is conservative by construction and preserves the mass to the machine precision. The performance of the method is also demonstrated by comparing the results obtained using the proposed finite volume method to those obtained using the well-established kinetic method.

© 2014 Elsevier Inc. All rights reserved.

* Corresponding author.
E-mail addresses: audusse@math.univ-paris13.fr (E. Audusse), fayssal@math.univ-paris13.fr (F. Benkhaldoun), sari@math.univ-paris13.fr (S. Sari), m.seaid@durham.ac.uk (M. Seaid), pablo.tassi@edf.fr (P. Tassi).

http://dx.doi.org/10.1016/j.jcp.2014.04.026
0021-9991/© 2014 Elsevier Inc. All rights reserved.

1. Introduction

Mathematical modeling of many types of water flows of stratified geophysical interest is based on the formulation and solution of the appropriate equations of continuity and motion of water. In general, free-surface flows represent a three-dimensional turbulent Newtonian flow in complicated geometrical domains with moving boundaries. The cost of incorporating three-dimensional data in natural water courses is often excessively high. Computational efforts needed to simulate three-dimensional turbulent free-surface flows can also be significant. In view of such considerations, many researchers have tended to use rational approximations in order to develop two-dimensional hydrodynamical models for shallow water flows. Indeed, under the influence of gravity, many free-surface water flows can be modeled by the well-established shallow water equations with the assumption that the vertical scale is much smaller than any typical horizontal scale. The shallow water equations can be derived from the non-stationary three-dimensional incompressible Navier–Stokes equations by averaging over a vertical coordinate using appropriate free-surface and boundary conditions and taking into consideration hydrostatic pressure distribution. It is expected that solutions of depth-averaged equations have similar properties as depth-averaged solutions of initial fluid equations. The shallow water equations in depth-averaged form have been successfully applied to many engineering problems and their application fields include a wide spectrum of phenomena other than water waves. For instance, the shallow water equations have applications in environmental and hydraulic engineering such as tidal flows in an estuary or coastal regions, rivers, reservoir and open channel flows. Such practical flow problems are not trivial to simulate since the geometry can be complex and the topography irregular but robust and efficient numerical techniques have been developed for the past fifteen years. Therefore, during the last decades, a first class of multi-layer shallow water models has been developed to handle flow problems involving superposition of immiscible shallow fluids. These fluids can differ in terms of density, compressibility and viscosity among others, see for instance [1,10–12,16,31]. The main advantage of these models is the fact that the multi-layer shallow water model avoids the expensive three-dimensional Navier–Stokes equations and obtains stratified horizontal flow velocities as the pressure distribution is nearly hydrostatic. Applying the same idea to a single fluid lead to the development of a second class of multi-layer models, see [3,6,7,14] among others. Both classes of multi-layered models have some links but contain also huge differences since for the second class the introduction of layers along the vertical direction is no more linked to the nature of the flow but it is a way to obtain a more accurate description of the flow than the classical shallow water equations. Depending on the choice of the definition of the layers, this second class of multi-layer models can be related to the so-called horizontal sigma or isopycnal coordinates that are commonly used for numerical solution of the hydrostatic Navier–Stokes equations. The main difference with these approaches however, lies in the use of extensions of robust finite volume schemes for hyperbolic systems developed in the context of classical shallow water equations. It also should be emphasized the fact that, for this second class of multi-layer models, the classical hypothesis on the shallowness of the flow is replaced by (i) the hydrostatic nature of the flow and (ii) the shallowness of the layers. Therefore, these models formally tend to the hydrostatic Navier–Stokes equations when the number of layers goes to infinity. It should also be pointed out that among the first class of multi-layer models (*i.e.* between pairs of nonmiscible materials), some authors recently introduced new models that handle with some mass exchange, see for example [19,20]. These models remain different from the models of the second class that are considered in the current study since the exchange takes place between physically distinguished materials.

A variety of modeling frameworks and computational schemes have been developed for the multi-layer shallow water flows. An early attempt to model the two-layer shallow equations was reported in [30] where a set of differential shallow water equations is formulated in a weak-interaction form. The computational method used in this reference consists of solving the surface and internal waves in different grids due to the order of magnitude difference in propagation speed between waves on the free surface and at the density interface. Two-layer shallow water flows have also been studied for example in [13] ignoring mixing between the layers. It has been shown that, due to the coupling of momentum between the layers which involves certain derivatives of the dependent variables, numerical schemes obtained by independent upwindings of each layer of the two-layer shallow water model are unconditionally unstable. Introducing a vertical partition of the water height, a first multi-layer shallow water system of isopycnal type was formally derived in [3] and numerically also solved using a kinetic scheme. A simpler multi-layer shallow water system of sigma-transform type was proposed in [7] accounting only for the total height of water and an average velocity per each layer as unknowns in the system. It has been shown that the model can be obtained by using a semi-discretization in the vertical direction of P_0 finite element types for the water velocity. In this case, the definition of the layers in the system does not correspond to a physical partition of the flow but is related to the quality of the desired approximation over the water velocity. This later multi-layered model is adopted in the present paper and numerically solved. Recently, a rigorous derivation of multi-layer shallow water equations has been presented in [14]. The essential difference between this class of models and the multi-layer shallow water models developed in [6,7] and adopted in the present study lies on the derivation of the viscous terms in the models. The authors in [14] derived the multi-layer model from the hydrostatic Navier–Stokes equations to obtain a fully justified viscosity tensor whereas, in [7] the multi-layer model is derived from the conventional Navier–Stokes equations using the shallow water assumption in the sense that some components of the viscosity tensor are very small and can be neglected. On the other hand, starting from the hydrostatic Euler equations multi-layer model is derived in [6] without considering the shallow water assumption and ad-hoc vertical and horizontal viscous terms are added a posteriori. We should point out that the viscous terms considered in the current model can be viewed as a simplified vertical viscosity used to impose local coupling between the layers while a fully detailed version of the viscous tensor in multi-layer shallow water equations are given in [14]. Needless

to mention that the emphasis in the present work is on the hyperbolic part of multi-layer shallow water equations which is the same in all the models developed in [6,7,14]. The main objective of this study is to develop a fast finite volume solver for multi-layered shallow water flows with mass exchange.

Numerical solution of the multi-layered shallow water equations often presents difficulties because of their nonlinearity, coupling between the free-surface equation and the equations governing the water flow, and bed complexity (compare [3,7, 29] among others). In addition, the difficulty in these models comes from the coupling terms involving some derivatives of the unknown physical variables that make the system non-conservative and eventually non-hyperbolic. Due to these terms, a numerical scheme originally designed for the conventional single-layer shallow water equations will lead to instabilities when it is applied to each layer separately. For the two-layer shallow water equations of the first class for nonmiscible fluids, the well-established Roe's scheme [25] has applied in [12] among others. Techniques based on central-upwind schemes using the surface elevation instead of the water depth have also been used in [18] for numerical solution of the two-layer shallow water equations for nonmiscible fluids. In [10] numerical methods based on kinetic reconstructions have been studied for these two-layer shallow water equations. In the framework of kinetic schemes, authors in [1] proposed a class of relaxation methods for solving two-layer shallow water equations for nonmiscible fluids. For solving multi-layered shallow water equations of the second type, the authors in [3,7] developed numerical methods based on kinetic reconstructions. However, the numerical dissipation is very excessive and for practical applications, this method may become computationally demanding due to its semi-implicit treatment of source terms. The well-established lattice Boltzmann method has also been extended to a class of multi-layered shallow water equations in [29], but the complexity of this method is relevant. For example, the optimal selection of relaxation rates and the numerical diffusion in this method are still a problem to overcome. In the present work we propose a new finite volume method of characteristics (FVC) to solve the multi-layered shallow water equations. The method has been first introduced and analyzed in [8] for the standard single-layer shallow water equations. The proposed FVC method avoids the solution of Riemann problems and belongs to the predictor–corrector type methods. The predictor stage uses the method of characteristics to reconstruct the numerical fluxes whereas the corrector stage recovers the conservation equations. The proposed method is simple, non-oscillatory and suitable for multi-layered shallow water equations for which Riemann problems are difficult to solve. It should be stressed that although the method uses the method of characteristics in its formulation, the overall solver is fully conservative by construction. The method of characteristics is only used later to compute the interface states at the control volumes to be used in the computation of numerical fluxes for the conservative finite volume solver. Numerical examples are presented to verify the considered multi-layered shallow water model. We demonstrate the method capability of calculating lateral and vertical distributions of velocities for dam-break and wind-driven circulation flows. Some results are presented as accuracy test examples and others, to the best of our knowledge, are reported for the first time.

The outline of this paper is as follows. We first give a brief description of the model employed for multi-layered shallow water flows in Section 2. In Section 3, we then formulate the finite volume method of characteristics for the multi-layered shallow water equations. This section includes the reconstruction of the numerical fluxes and the discretization of source terms. Numerical results are presented in Section 4. Conclusions are summarized in Section 5.

2. Multi-layered shallow water equations

The governing equations for multi-layered shallow water flows with mass exchange can be derived from the three-dimensional hydrostatic incompressible Navier–Stokes equations with free surface by considering a vertical P_0 type discretization of the horizontal velocity. This vertical discretization defines a series of layers in the flow domain and the equations are vertically integrated on each layer separately, compare [3,6,7,14] for a detailed discussion on the derivation of these models. It should be pointed out that the layers defined in the model do not refer to physical interfaces between non-miscible fluids but to a meshless discretization of the flow domain. Hence, the possibility of water exchange between the layers is accounted for in the model. The great interest of this strategy is to preserve an accurate description of the velocity profile but to deal with a two-dimensional fluid model and thus to avoid the difficult drawback of meshing a three-dimensional moving domain for which the free-surface may present very sharp profiles such as dam-break problems and hydraulic jumps. In the current study, we consider the one-dimensional version of the model written in a conservative form as

$$\begin{aligned} &\frac{\partial H}{\partial t} + \sum_{\alpha=1}^{M} \frac{\partial}{\partial x}(l_\alpha H u_\alpha) = 0, \\ &\frac{\partial}{\partial t}(l_\alpha H u_\alpha) + \frac{\partial}{\partial x}\left(l_\alpha H u_\alpha^2 + \frac{1}{2} g l_\alpha H^2\right) = -g l_\alpha H \frac{\partial Z}{\partial x} + F_\alpha, \end{aligned} \tag{1}$$

where $u_\alpha(t,x)$ is the local water velocity for the αth layer, $Z(x)$ the topography of the basin, g the gravitational acceleration, $H(t,x)$ denotes the water height of the whole flow system and l_α denotes the relative size of the αth layer with

$$l_\alpha > 0, \quad \sum_{\alpha=1}^{M} l_\alpha = 1.$$

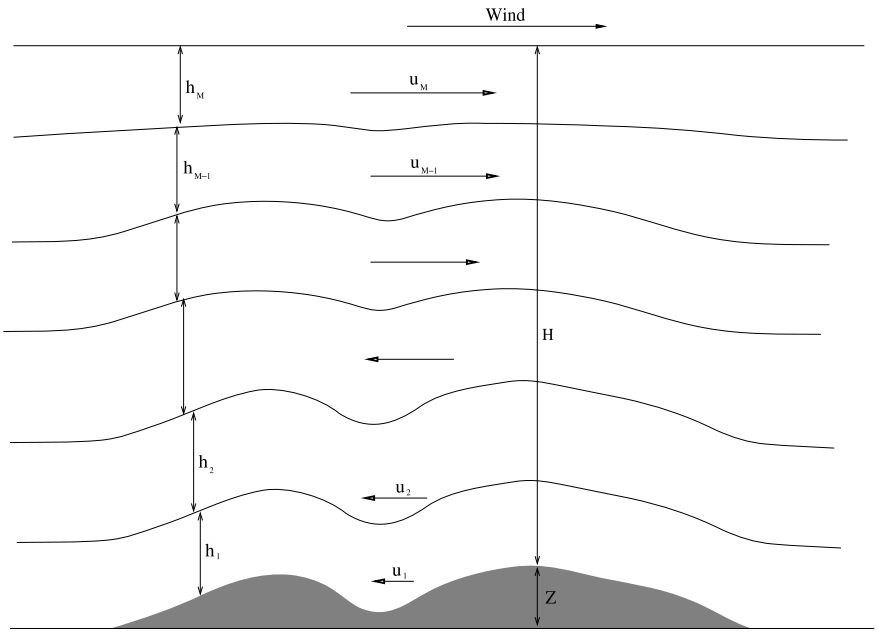


Fig. 1. Schematic of a multi-layered shallow water system.

The water height $h_\alpha(t,x)$ of the αth layer is defined as

$$h_\alpha = l_\alpha H, \quad \alpha = 1,\dots,M,$$

where M is the total number of layers in the flow domain, see Fig. 1 for an illustration. In (1), the source term F_α is the external force acting on the layer α and accounting for the friction and momentum exchange effects. Thus,

$$F_\alpha = \mathcal{F}_u + \mathcal{F}_b + \mathcal{F}_w + \mathcal{F}_\mu, \quad \alpha = 1,2,\dots,M, \tag{2}$$

where the first term $\mathcal{F}_u$ is related to the momentum exchanges between the layers that are defined through the vertical P_0 discretization of the flow. The three last terms $\mathcal{F}_b$, $\mathcal{F}_w$ and $\mathcal{F}_\mu$ are related to friction effects. Note that the bed friction forcing term $\mathcal{F}_b$ is acting only on the lower layer, whereas the wind-driven forcing term $\mathcal{F}_w$ is acting only on the upper layer. The internal friction term $\mathcal{F}_\mu$ models the friction between neighboring layers, see [3] for further details. Thus, the advection term $\mathcal{F}_u$ is given by

$$\mathcal{F}_u = u_{\alpha+1/2}G_{\alpha+1/2} - u_{\alpha-1/2}G_{\alpha-1/2}, \tag{3}$$

where the mass exchange terms $G_{\alpha+1/2}$ can be computed as

$$G_{\alpha+1/2} = \sum_{\beta=1}^{\alpha}\left(\frac{\partial(h_\beta u_\beta)}{\partial x} - l_\beta \sum_{\gamma=1}^{M}\frac{\partial(h_\gamma u_\gamma)}{\partial x}\right), \quad \alpha = 1,2,\dots,M-1, \tag{4}$$

with

$$G_{1/2} = G_{M+1/2} = 0,$$

and the interface velocity is computed by a simple upwinding following the sign of the mass exchange term as

$$u_{\alpha+1/2} = \begin{cases} u_\alpha, & \text{if } G_{\alpha+1/2} \geq 0, \\ u_{\alpha+1}, & \text{if } G_{\alpha+1/2} < 0. \end{cases} \tag{5}$$

Note that the mass exchange terms $G_{\alpha+1/2}$ can be interpreted as the sum over all layers lower than the considered layer l_α of the difference between the water discharge of each layer and the weighted total discharge at the same point. The vertical kinematic eddy viscosity term $\mathcal{F}_\mu$ takes into account the friction between neighboring layers and it is defined as

$$\mathcal{F}_\mu = 2\nu(1-\delta_{M\alpha})\frac{u_{\alpha+1}-u_\alpha}{(l_{\alpha+1}+l_\alpha)H} - 2\nu(1-\delta_{1\alpha})\frac{u_\alpha - u_{\alpha-1}}{(l_\alpha + l_{\alpha-1})H}, \tag{6}$$

where ν is the eddy viscosity and $\delta_{k\alpha}$ represents the Kronecker delta defined as

$$\delta_{k\alpha} = \begin{cases} 1, & \text{if } k = \alpha, \\ 0, & \text{if } k \neq \alpha. \end{cases}$$

Notice that a general derivation of the viscous tensor in multi-layer shallow water equations can be found in [14]. The external friction terms are given by

$$\mathcal{F}_b = -\delta_{1\alpha}\frac{\tau_b}{\rho}, \qquad \mathcal{F}_w = \delta_{M\alpha}\frac{\tau_w}{\rho}, \tag{7}$$

with ρ is the water density, τ_b and τ_w are respectively, the bed shear stress and the shear of the blowing wind defined by the water velocity u_1 and the wind velocity w as

$$\tau_b = \rho C_b u_1 |u_1|, \qquad \tau_w = \rho C_w w|w|, \tag{8}$$

where C_b is the bed friction coefficient, which may be either constant or estimated as

$$C_b = \frac{g n_b^2}{H^{1/3}},$$

with n_b being the Manning roughness coefficient at the bed, w is the wind velocity at 10 m above the water surface and C_w is the wind friction coefficient defined as [27]

$$C_w = \frac{\sigma^2 \rho_a}{H},$$

where σ^2 is the wind stress coefficient and ρ_a is the air density. For simplicity in the presentation we rewrite Eqs. (1) in a compact vector form as

$$\frac{\partial \mathbf{W}}{\partial t} + \frac{\partial \mathbf{F}(\mathbf{W})}{\partial x} = \mathbf{Q}(\mathbf{W}) + \mathbf{R}(\mathbf{W}), \tag{9}$$

where $\mathbf{W}$ is the vector of conserved variables, $\mathbf{F}$ the vector of flux functions, $\mathbf{Q}$ and $\mathbf{R}$ are the vector of source terms

$$\mathbf{W} = \begin{pmatrix} H \\ Hu_1 \\ Hu_2 \\ \vdots \\ Hu_M \end{pmatrix}, \qquad \mathbf{F}(\mathbf{W}) = \begin{pmatrix} \sum_{\alpha=1}^{M} l_\alpha H u_\alpha \\ Hu_1^2 + \frac{1}{2}gH^2 \\ Hu_2^2 + \frac{1}{2}gH^2 \\ \vdots \\ Hu_M^2 + \frac{1}{2}gH^2 \end{pmatrix}, \qquad \mathbf{Q}(\mathbf{W}) = \begin{pmatrix} 0 \\ -gH\frac{\partial Z}{\partial x} \\ -gH\frac{\partial Z}{\partial x} \\ \vdots \\ -gH\frac{\partial Z}{\partial x} \end{pmatrix},$$

$$\mathbf{R}(\mathbf{W}) = \begin{pmatrix} 0 \\ \frac{1}{l_1}\left(u_{3/2}G_{3/2} - \frac{\tau_b}{\rho} + 2\nu\frac{u_2-u_1}{(l_2+l_1)H}\right) \\ \frac{1}{l_2}\left(u_{5/2}G_{5/2} - u_{3/2}G_{3/2} + 2\nu\frac{u_3-u_2}{(l_3+l_2)H} - 2\nu\frac{u_2-u_1}{(l_2+l_1)H}\right) \\ \vdots \\ \frac{1}{l_{M-1}}\left(u_{M-1/2}G_{M-1/2} - u_{M-3/2}G_{M-3/2} + 2\nu\frac{u_M-u_{M-1}}{(l_M+l_{M-1})H} - 2\nu\frac{u_{M-1}-u_{M-2}}{(l_{M-1}+l_{M-2})H}\right) \\ \frac{1}{l_M}\left(-u_{M-1/2}G_{M-1/2} + \frac{\tau_w}{\rho} - 2\nu\frac{u_M-u_{M-1}}{(l_M+l_{M-1})H}\right) \end{pmatrix}.$$

Note that the passage from Eqs. (1) to the system (9) has been achieved by dividing the second equation in (1) by l_α. Notice that Eqs. (9) have to be solved in a bounded spatial domain equipped with given boundary and initial conditions. In practice, these conditions are problem dependent and their discussion is postponed for Section 4 where numerical results will be discussed.

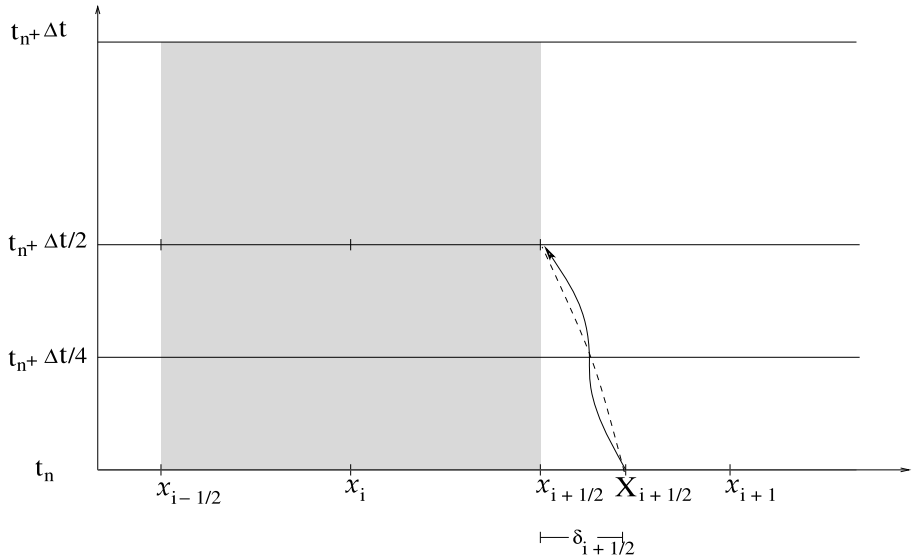


Fig. 2. A schematic diagram showing the control volumes and the main quantities used in the calculation of the departure points. The exact trajectory is represented by a solid line and the approximate trajectory with a dashed line.

3. Finite volume method of characteristics

It is evident that the calculation of the eigenvalues associated with the multi-layered system (9) is not trivial and there exist flow situations where these eigenvalues do not remain real. In these cases, the system is not hyperbolic and yields to the so-called Kelvin–Helmholtz instability at the interface separating the layers. In the current study, the proposed finite volume method of characteristics does not require the calculation of the eigenvalues for the multi-layered system and can be applied for any arbitrary number M of the layers in the system. It is worth remarking that an estimation of the eigenvalues in the multi-layered model (9) may be used for controlling the timestep size in the numerical simulation. To this end, we use the eigenvalues associated with the single-layer shallow water counterparts defined as

$$\lambda_\alpha^{\pm} = u_\alpha \pm \sqrt{gH}, \quad \alpha = 1, 2, \ldots, M. \tag{10}$$

Note that the approximation (10) can simply be replaced by the maximum wave speed for the multi-layer shallow water equations. In what follows we describe the different steps of the proposed finite volume method of characteristics to solve the multi-layered shallow water equations (9).

3.1. Time integration procedure

Let us discretize the spatial domain into control volumes $[x_{i-1/2}, x_{i+1/2}]$ with uniform size $\Delta x = x_{i+1/2} - x_{i-1/2}$ and divide the temporal domain into subintervals $[t_n, t_{n+1}]$ with stepsize Δt. Here, $t_n = n\Delta t$, $x_{i-1/2} = i\Delta x$ and $x_i = (i + 1/2)\Delta x$ is the center of the control volume. Integrating Eq. (9) with respect to space over the control volume $[x_{i-1/2}, x_{i+1/2}]$ shown in Fig. 2, we obtain the following semi-discrete equations

$$\frac{d\mathbf{W}_i}{dt} + \frac{\mathcal{F}_{i+1/2} - \mathcal{F}_{i-1/2}}{\Delta x} = \mathcal{Q}_i + \mathcal{R}_i, \tag{11}$$

where $\mathbf{W}_i(t)$ is the space average of the solution $\mathbf{W}$ in the control volume $[x_{i-1/2}, x_{i+1/2}]$ at time t, *i.e.*,

$$\mathbf{W}_i(t) = \frac{1}{\Delta x} \int_{x_{i-1/2}}^{x_{i+1/2}} \mathbf{W}(t, x)\, dx,$$

and $\mathcal{F}_{i\pm1/2} = \mathbf{F}(\mathbf{W}_{i\pm1/2})$ are the numerical fluxes at $x = x_{i\pm1/2}$ and time t. In (11), $\mathcal{Q}_i$ and $\mathcal{R}_i$ are the difference notation for the discretized source terms $\mathbf{Q}(\mathbf{W}_i)$ and $\mathbf{R}(\mathbf{W}_i)$ in (9), respectively. To integrate the system (11) in time we consider an operator splitting method consisting first of the predictor step

$$\mathbf{W}_i^* = \mathbf{W}_i^n + \Delta t \mathcal{R}_i^n, \tag{12}$$

followed by the corrector step

$$\mathbf{W}_i^{n+1} = \mathbf{W}_i^* - \Delta t \frac{\mathcal{F}^*_{i+1/2} - \mathcal{F}^*_{i-1/2}}{\Delta x} + \Delta t \mathcal{Q}_i^*. \tag{13}$$

It should be pointed out that as with all explicit time stepping methods the theoretical maximum stable time step Δt is specified according to the Courant–Friedrichs–Lewy (CFL) condition

$$\Delta t = Cr \frac{\Delta x}{\max_{\alpha=1,\dots,M}(|\lambda_\alpha^n|)}, \tag{14}$$

where Cr is the Courant number to be chosen less than unity. Note that we have used the eigenvalues of the single-layer model (10) to control the time step in (14). However, one could use a fixed time step or a rough estimation of the eigenvalues for the multi-layer model. In practice, if the explicit expression of the eigenvalues is available, the stability condition (14) could be changed to include these eigenvalues. It should also be stressed that for stability reasons an upper bound of the eigenvalues should appear in (14) and not an estimation of the eigenvalues of the single-layer model. However, all the numerical results presented in the present work suggest that the CFL condition (14) ensures the stability of the proposed method.

The spatial discretization of Eq. (13) is complete when a numerical construction of the numerical fluxes $\mathcal{F}^*_{i\pm1/2}$ and source terms $\mathcal{Q}_i^*$ are chosen. In general, the construction of the numerical fluxes requires a solution of Riemann problems at the interfaces $x_{i\pm1/2}$, see for example [2,25]. From a computational viewpoint, this procedure is very demanding and may restrict the application of the method for which Riemann solutions are not available. Our objective in the present work is to present a class of finite volume method of characteristics (FVC) that is simple, easy to implement, and accurately solves Eqs. (9) without relying on Riemann problem solvers or complicated techniques for well-balancing the discretizations of the gradient fluxes and the source terms. This objective is reached by reformulating the multi-layered system in an advective form and integrating the obtained system along the characteristics defined by the advection velocity.

3.2. Discretization of the flux gradients

To reconstruct the numerical fluxes $\mathcal{F}^n_{i\pm1/2}$ in (13), we consider the method of characteristics applied to an advective version of the system (1). In practice, the advective form of the multi-layered shallow water equations (9) is built such that the non-conservative variables are transported with a velocity field associated with each layer. Here, the multi-layered shallow water equations (9), without accounting for the source term $\mathbf{R}(\mathbf{W})$, are reformulated in an advective form as

$$\begin{aligned} &\frac{\partial H}{\partial t} + \left(\sum_{\alpha=1}^{M} l_\alpha u_\alpha\right)\frac{\partial H}{\partial x} = -\sum_{\alpha=1}^{M} l_\alpha H \frac{\partial u_\alpha}{\partial x}, \\ &\frac{\partial q_\alpha}{\partial t} + u_\alpha \frac{\partial q_\alpha}{\partial x} = -q_\alpha \frac{\partial u_\alpha}{\partial x} - gH\frac{\partial}{\partial x}(H+Z), \end{aligned} \tag{15}$$

which can be rearranged in a compact form as

$$\frac{\partial U_\alpha}{\partial t} + \mathcal{U}_\alpha \frac{\partial U_\alpha}{\partial x} = S_\alpha(\mathbf{U}), \quad \alpha = 0, 1, \dots, M, \tag{16}$$

where $q_\alpha = Hu_\alpha$ is the water discharge, $\mathbf{U} = (U_0, U_1, \dots, U_M)^T$, $\mathbf{S}(\mathbf{U}) = (S_0, S_1, \dots, S_M)^T$ with

$$\mathbf{U} = \begin{pmatrix} H \\ q_1 \\ q_2 \\ \vdots \\ q_M \end{pmatrix}, \qquad \mathbf{S}(\mathbf{U}) = \begin{pmatrix} -\sum_{\alpha=1}^{M} l_\alpha H \frac{\partial u_\alpha}{\partial x} \\ -Hu_1 \frac{\partial u_1}{\partial x} - gH\frac{\partial}{\partial x}(H+Z) \\ -Hu_2 \frac{\partial u_2}{\partial x} - gH\frac{\partial}{\partial x}(H+Z) \\ \vdots \\ -Hu_M \frac{\partial u_M}{\partial x} - gH\frac{\partial}{\partial x}(H+Z) \end{pmatrix},$$

and the advection velocity $\mathcal{U}_\alpha$ is defined as

$$\mathcal{U}_\alpha = \begin{cases} \sum_{\beta=1}^{M} l_\beta u_\beta, & \text{if } \alpha = 0, \\ u_\alpha, & \text{if } \alpha = 1, 2, \dots, M. \end{cases} \tag{17}$$

Note that the case with $\alpha = 0$ does not refer to any layer in the system but to the global mass equation. It is only used here to formulate the compact advective form (16) for the whole system. The fundamental idea of the method of characteristics is to impose a regular grid at the new time level and to backtrack the flow trajectories to the previous time level. At the

old time level, the quantities that are needed are evaluated by interpolation from their known values on a regular grid. For more discussions we refer the reader to [24,26,28] among others. Thus, the characteristic curves associated with Eq. (16) are solutions of the initial-value problems

$$\begin{aligned}&\frac{dX_{\alpha,i+1/2}(\tau)}{d\tau} = \mathcal{U}_{\alpha,i+1/2}\big(\tau, X_{\alpha,i+1/2}(\tau)\big), \quad \tau \in [t_n, t_n + \Delta t/2],\\ &X_{\alpha,i+1/2}(t_n + \Delta t/2) = x_{i+1/2}, \quad \alpha = 0, 1, \ldots, M.\end{aligned} \tag{18}$$

Note that $X_{\alpha,i+1/2}(\tau)$ are the departure points at time τ of a particle that will arrive at the gridpoint $x_{i+1/2}$ in time $t_n + \Delta t/2$. The method of characteristics does not follow the flow particles forward in time, as the Lagrangian schemes do, instead it traces backward the position at time t_n of particles that will reach the points of a fixed mesh at time $t_n + \Delta t/2$. By doing so, the method avoids the grid distortion difficulties that the conventional Lagrangian schemes have, see for instance [23,24,28] and further references are therein. The solutions of (18) can be expressed as

$$\begin{aligned}X_{\alpha,i+1/2}(t_n) &= x_{i+1/2} - \int_{t_n}^{t_n+\Delta t/2} \mathcal{U}_{\alpha,i+1/2}\big(X_{\alpha,i+1/2}(\tau)\big)d\tau,\\ &= x_{i+1/2} - \delta_{\alpha,i+1/2}.\end{aligned} \tag{19}$$

To approximate the integral in (19), we used a method first proposed in the context of semi-Lagrangian schemes to integrate the weather prediction equations in [28]. Note that $\delta_{\alpha,i+1/2}$ denotes the displacement between a mesh point on the new level, $x_{i+1/2}$, and the departure point of the trajectory to this point on the previous time level $X_{\alpha,i+1/2}(t_n)$, *i.e.*

$$\delta_{\alpha,i+1/2} = x_{i+1/2} - X_{\alpha,i+1/2}(t_n).$$

Applying the mid-point rule to approximate the integral in (19) yields

$$\delta_{\alpha,i+1/2} = \frac{\Delta t}{2}\mathcal{U}_{\alpha,i+1/2}\big(t_{n+1/2}, X_{\alpha,i+1/2}(t_{n+1/2})\big). \tag{20}$$

Using the second-order extrapolation

$$\mathcal{U}_{\alpha,i+1/2}(t_{n+1/2}, x_{i+1/2}) = \frac{3}{2}\mathcal{U}_{\alpha,i+1/2}(t_n, x_{i+1/2}) - \frac{1}{2}\mathcal{U}_{\alpha,i+1/2}(t_{n-1}, x_{i+1/2}), \tag{21}$$

and the second-order approximation

$$X_{\alpha,i+1/2}(t_{n+1/2}) = x_{i+1/2} - \frac{1}{2}\delta_{\alpha,i+1/2},$$

we obtain the following implicit formula for $\delta_{\alpha,i+1/2}$

$$\delta_{\alpha,i+1/2} = \frac{\Delta t}{2}\left[\frac{3}{2}\mathcal{U}_{\alpha,i+1/2}\left(t_n, x_{i+1/2} - \frac{1}{2}\delta_{\alpha,i+1/2}\right) - \frac{1}{2}\mathcal{U}_{\alpha,i+1/2}\left(t_{n-1}, x_{i+1/2} - \frac{1}{2}\delta_{\alpha,i+1/2}\right)\right].$$

To compute $\delta_{\alpha,i+1/2}$ we consider the following successive iteration procedure

$$\begin{aligned}\delta^{(0)}_{\alpha,i+1/2} &= \frac{\Delta t}{2}\left[\frac{3}{2}\mathcal{U}_{\alpha,i+1/2}(t_n, x_{i+1/2}) - \frac{1}{2}\mathcal{U}_{\alpha,i+1/2}(t_{n-1}, x_{i+1/2})\right],\\ \delta^{(k)}_{\alpha,i+1/2} &= \frac{\Delta t}{2}\left[\frac{3}{2}\mathcal{U}_{\alpha,i+1/2}\left(t_n, x_{i+1/2}\frac{1}{2}\delta^{(k-1)}_{\alpha,i+1/2}\right)\right]\\ &\quad - \frac{\Delta t}{2}\left[\frac{1}{2}\mathcal{U}_{\alpha,i+1/2}\left(t_{n-1}, x_{i+1/2} - \frac{1}{2}\delta^{(k-1)}_{\alpha,i+1/2}\right)\right], \quad k = 1, 2, \ldots.\end{aligned} \tag{22}$$

The iterations (22) are terminated when the following criteria

$$\frac{\|\delta^{(k)}_\alpha - \delta^{(k-1)}_\alpha\|}{\|\delta^{(k-1)}_\alpha\|} \le \varepsilon, \tag{23}$$

is fulfilled for the L^∞-norm $\|\cdot\|$ and a given tolerance ε. It is also known [23] that

$$\left\|\delta_\alpha - \delta^{(k)}_\alpha\right\| \le \frac{\Delta t}{4}\left\|\delta_\alpha - \delta^{(k-1)}_\alpha\right\| \max_{\alpha=0,1,\ldots,M}\left|\frac{\partial \mathcal{U}_\alpha}{\partial x}\right|, \quad k = 1, 2, \ldots. \tag{24}$$

Hence, a sufficient condition for the convergence of iterations (22) is that the velocity gradient satisfies

$$\max_{\alpha=0,1,\ldots,M}\left|\frac{\partial \mathcal{U}_\alpha}{\partial x}\right|\frac{\Delta t}{4}\leq 1. \tag{25}$$

Note that the condition (25) is sufficient to guarantee that the characteristic curves do not intersect during a time step of size $\Delta t/2$. Furthermore, if $|\frac{\partial \mathcal{U}_\alpha}{\partial x}|\Delta t$ is sufficiently small, we can conclude that a few iterations (1 or 2) are enough to approximate the characteristic curves up to $\mathcal{O}((\Delta t)^3)$, see [23,26,28] among others. In all numerical results presented in this study, the number of iterations in (22) to reach a tolerance of $\varepsilon = 10^{-6}$ does not exceed 1 iteration. This is mainly due to the small hyperbolic Courant number used in the simulations. For the considered test examples in Section 4, we have found that it suffices that the hyperbolic CFL condition (14) is satisfied to ensure convergence in the iterations (22). A schematic representation of the quantities involved in computing the departure points is shown in Fig. 2.

Once the characteristics curves $X_{\alpha,i+1/2}(t_n)$ are known, a solution at the cell interface $x_{i+1/2}$ is reconstructed as

$$\mathbf{U}^{n+1/2}_{\alpha,i+1/2} = \mathbf{U}_\alpha(t_n+\Delta t/2, x_{i+1/2}) = \widetilde{\mathbf{U}}_\alpha\big(t_n, X_{\alpha,i+1/2}(t_n)\big), \tag{26}$$

where $\widetilde{\mathbf{U}}_\alpha(t_n, X_{\alpha,i+1/2}(t_n))$ is the solution at the characteristic foot computed by interpolation from the gridpoints of the control volume where the departure point resides *i.e.*

$$\widetilde{\mathbf{U}}_\alpha\big(t_n, X_{\alpha,i+1/2}(t_n)\big) = \mathcal{P}\big(\mathbf{U}_\alpha\big(t_n, X_{\alpha,i+1/2}(t_n)\big)\big), \tag{27}$$

where $\mathcal{P}$ represents an interpolating polynomial. For instance, a Lagrange-based interpolation polynomials can be formulated as

$$\mathcal{P}\big(\mathbf{U}_j\big(t_n, X_{\alpha,i+1/2}(t_n)\big)\big) = \sum_k \mathcal{L}_k(X_{\alpha,i+1/2})\mathbf{U}^n_{\alpha,k}, \tag{28}$$

with $\mathcal{L}_k$ being the Lagrange basis polynomials given by

$$\mathcal{L}_k(x) = \prod_{\substack{k'=0\\ k'\neq k}} \frac{x-x_{k'}}{x_k-x_{k'}}.$$

Note that other interpolation procedures such as Spline or Hermite interpolation methods or interpolation techniques based on radial basis functions can also be applied in (27). It is worth mentioning that the proposed finite volume method is fully conservative by construction and the non-conservative system (15) is used only to compute the intermediate states for the numerical fluxes in (11).

3.3. Discretization of the source terms

Applied to Eqs. (16), the characteristic solutions are given by

$$\begin{aligned}
H^{n+1/2}_{i+1/2} &= \widetilde{H}^{n+1/2}_{i+1/2} - \frac{\Delta t}{2\Delta x}\widetilde{H}^{n+1/2}_{i+1/2}\sum_{\alpha=1}^{M} l_\alpha\big(u^{n+1/2}_{\alpha,i+1} - u^{n+1/2}_{\alpha,i}\big),\\
q^{n+1/2}_{\alpha,i+1/2} &= \widetilde{q}^{n+1/2}_{\alpha,i+1/2} - \frac{\Delta t}{2\Delta x}\Big(\widetilde{q}^{n+1/2}_{\alpha,i+1/2}\big(u^{n+1/2}_{\alpha,i+1} - u^{n+1/2}_{\alpha,i}\big)\\
&\qquad + g\widetilde{H}^{n+1/2}_{i+1/2}\big(\big(H^{n+1/2}_{i+1} + Z^n_{i+1}\big) - \big(H^{n+1/2}_i + Z^n_i\big)\big)\Big),
\end{aligned} \tag{29}$$

where

$$\widetilde{H}^{n+1/2}_{i+1/2} = H\big(t_n, X_{0,i+1/2}(t_n)\big), \qquad \widetilde{q}^{n+1/2}_{\alpha,i+1/2} = q_\alpha\big(t_n, X_{\alpha,i+1/2}(t_n)\big),$$

are the solutions at the characteristic foot computed by interpolation from the gridpoints of the control volume where the departure points $X_{\alpha,i+1/2}(t_n)$ belong. The numerical fluxes $\mathcal{F}_{i\pm1/2}$ in (11) are calculated using the intermediate states $\mathbf{W}^{n+1/2}_{i\pm1/2}$ recovered accordingly from the characteristic solutions $\mathbf{U}^{n+1/2}_{j,i\pm1/2}$ in (26). Hence, the corrector stage (13) in the FVC method reduces to

$$\begin{aligned}
H^{n+1}_i &= H^{n+1/2}_i - \frac{\Delta t}{\Delta x}\sum_{\alpha=1}^{M}\big((l_\alpha H u_\alpha)^{n+1/2}_{i+1/2} - (l_\alpha H u_\alpha)^{n+1/2}_{i-1/2}\big),\\
q^{n+1}_{\alpha,i} &= q^{n+1/2}_{\alpha,i} - \frac{\Delta t}{\Delta x}\left(\left(Hu^2_\alpha + \frac{1}{2}gH^2\right)^{n+1/2}_{i+1/2} - \left(Hu^2_\alpha + \frac{1}{2}gH^2\right)^{n+1/2}_{i-1/2}\right)\\
&\qquad - \frac{\Delta t}{\Delta x}g\widehat{H}^{n+1/2}_i\big(Z^n_{i+1} - Z^n_{i-1}\big).
\end{aligned} \tag{30}$$

In our FVC method, the reconstruction of the term $\widehat{H}_i^{n+1/2}$ in (30) is carried out such that the discretization of the source terms is well balanced with the discretization of flux gradients using the concept of C-property [9]. Here, a numerical scheme is said to satisfy the C-property for Eqs. (9) if the condition

$$Z + H^n = C, \qquad u_\alpha^n = 0, \quad \alpha = 1, \dots, M, \tag{31}$$

holds for stationary flows at rest. In (31), C is a positive constant. Therefore, the treatment of source terms in (30) is reconstructed such that the condition (31) is preserved at the discrete level.

Let us assume a stationary flow at rest, $u_\alpha = 0$, $\alpha = 1, 2, \dots, M$, and a linear interpolation procedure is used in the FVC method. Thus, the system (9) reduces to

$$\frac{\partial}{\partial t}\begin{pmatrix} H \\ 0 \end{pmatrix} + \frac{\partial}{\partial x}\begin{pmatrix} 0 \\ \frac{1}{2}gH^2 \end{pmatrix} = \begin{pmatrix} 0 \\ -gH\frac{\partial Z}{\partial x} \end{pmatrix}. \tag{32}$$

Applied to the system (32), the stage (29) computes

$$\begin{aligned} H_{i+1/2}^{n+1/2} &= \frac{H_i^{n+1/2} + H_{i+1}^{n+1/2}}{2}, \\ u_{\alpha,i+1/2}^n &= 0, \quad \alpha = 1, \dots, M, \end{aligned} \tag{33}$$

while the stage (30) updates the solution as

$$\begin{aligned} H_i^{n+1} &= H_i^{n+1/2}, \\ q_{\alpha,i}^{n+1} &= q_{\alpha,i}^{n+1/2} - \frac{1}{2}\frac{\Delta t}{\Delta x} g\big((H_{i+1/2}^{n+1/2})^2 - (H_{i-1/2}^{n+1/2})^2\big) - \Delta t g\left(H\frac{\partial Z}{\partial x}\right)_i^{n+1/2}. \end{aligned} \tag{34}$$

To obtain stationary solutions $H_i^{n+1} = H_i^n$, the sum of discretized flux gradient and source term in (34) should be equal to zero *i.e.*,

$$\frac{1}{2\Delta x}\big((H_{i+1/2}^{n+1/2})^2 - (H_{i-1/2}^{n+1/2})^2\big) = -\left(H\frac{\partial Z}{\partial x}\right)_i^{n+1/2}. \tag{35}$$

Using $H_{i+1/2}^{n+1/2} = \frac{H_i^{n+1/2} + H_{i+1}^{n+1/2}}{2}$, the condition (35) is equivalent to

$$\frac{1}{8\Delta x}\big(H_{i+1}^{n+1/2} + 2H_i^n + H_{i-1}^{n+1/2}\big)\big(H_{i+1}^{n+1/2} - H_{i-1}^{n+1/2}\big) = -\left(H\frac{\partial Z}{\partial x}\right)_i^{n+1/2}. \tag{36}$$

Since for stationary solutions $H_{i+1}^{n+1/2} - H_{i-1}^{n+1/2} = Z_{i+1} - Z_{i-1}$, Eqs. (36) become

$$\left(H\frac{\partial Z}{\partial x}\right)_i^{n+1/2} = \frac{H_{i+1/2}^{n+1/2} + H_{i-1/2}^{n+1/2}}{2}\frac{Z_{i+1} - Z_{i-1}}{2\Delta x}. \tag{37}$$

Hence, if the source term $\widehat{H}_i^{n+1/2}$ in the predictor stage (30) is discretized as

$$\widehat{H}_i^{n+1/2} = \frac{1}{4}\big(H_{i+1}^{n+1/2} + 2H_i^{n+1/2} + H_{i-1}^{n+1/2}\big), \tag{38}$$

then the proposed FVC method satisfies the C-property. A detailed analysis of convergence and stability has been presented in [8] for nonlinear scalar problems. Notice that this property is achieved by assuming a linear interpolation procedure in the predictor stage of the FVC method. However, a well-balanced discretization of flux gradients and source terms for a quadratic or cubic interpolation procedures can be carried out using similar techniques.

In summary, the implementation of FVC algorithm to solve the multi-layered shallow water equations (9) is carried out in the following steps. Given the solution $(H_i^n, q_{\alpha,i}^n)$ at time t_n, we compute the solution $(H_i^{n+1}, q_{\alpha,i}^{n+1})$ at the next time level t_{n+1} via:

Step 1. *Perform the first step of the time splitting in (12) to compute the solutions H_i^* and $q_{\alpha,i}^*$, $\alpha = 1, 2, \dots, M$.*
Step 2. *Compute the departure points $X_{\alpha,i+1/2}(t_n)$, with $\alpha = 0, 1, \dots, M$ using for example the iterative procedure (22).*
Step 3. *Compute the approximations*

$$\widetilde{H}_{i+1/2}^n = H\big(t_n, X_{0,i+1/2}(t_n)\big) \quad \text{and} \quad \widetilde{q}_{\alpha,i+1/2}^n = q_\alpha\big(t_n, X_{\alpha,i+1/2}(t_n)\big), \quad \alpha = 1, \dots, M$$

employing an interpolation procedure.

Step 4. *Evaluate the intermediate states* $H_{i+1/2}^{n+1/2}$ *and* $q_{\alpha,i+1/2}^{n+1/2}$, $\alpha = 1, \ldots, M$ *from the predictor stage (29).*

Step 5. *Update the solutions* H_i^{n+1} *and* $q_{\alpha,i}^{n+1}$, $\alpha = 1, \ldots, M$ *using the corrector stage (30).*

Note that several interpolation procedures can be applied in step 3. In the current study we have used a linear interpolation since for this type of interpolations the obtained solution remains monotone and the FVC method preserves the exact C-property at the machine precision, compare for example [8].

4. Numerical results and examples

We present numerical results for several test problems in shallow water flows to check the accuracy and the performance of the proposed multi-layered finite volume model. We first examine the conservation property of the FVC scheme and then we compare the obtained results for a dam-break problem to those obtained using the three-dimensional Navier–Stokes equations. We also solve a class of wind-driven circulation problems in closed water channels and the obtained velocity profiles are compared to those analytically calculated [27]. The FVC results are also compared to numerical results obtained using the kinetic scheme developed in [7] to solve the multi-layer shallow water equations. Details on the implementation of this kinetic scheme can be found in [5,22] and are omitted here.

In this section we also compare the numerical results obtained using the proposed multi-layered finite volume method to those obtained using a three-dimensional model for free-surface flows. The considered 3D numerical code belongs to the open source TELEMAC-3D,[1] which solves the 3D Navier–Stokes equations using a finite element discretization under hydrostatic or non-hydrostatic approximations, compare [17] for more details. The hydrostatic approximation consists on neglecting the vertical acceleration, diffusion and source terms in the momentum equations. The non-hydrostatic approximation is based on the pressure decomposition into hydrostatic and hydrodynamic parts, allowing an accurate computation of the vertical velocity, which is now coupled with the whole system of equations. The overall algorithm for the solution of the hydrostatic 3D model is given hereafter: (i) computation of the advected velocity components by solving the advection terms in the momentum equations; (ii) determination of the new velocity components by taking into account the diffusion and source terms in the momentum equations (intermediate velocity field); (iii) computation of the water depth from vertical integration of the continuity equation and momentum equations by excluding the pressure terms; and (iv) determination of the vertical velocity from the continuity equation and computation of the pressure step by the well-established projection method. The overall algorithm for the solution of the 3D non-hydrostatic model can be summarized as: (i) a hydrostatic part, which is almost exactly to the hydrostatic model described above, with the exception that the vertical velocity is also advected and diffused. In this step the free surface function is also determined; and (ii) a non-hydrostatic part, in which the velocity field is corrected by the dynamic pressure gradients in order to fulfill the divergence-free constraint. The computations presented in the current study were performed using the non-hydrostatic approximation. For the mesh generation, the 3D finite element mesh is obtained by first dividing the two-dimensional domain with non-overlapping linear triangles and then by extruding each triangle along the vertical direction into linear prismatic columns that exactly fit the bottom and the free-surface. In doing so, each column can be partitioned into non-overlapping layers, requiring that two adjacent layers comprise the same number of prisms. Turbulent stresses and turbulent fluxes are modeled using turbulent viscosity and turbulent gradient diffusion hypothesis, which respectively introduce eddy viscosity and eddy diffusivity. Several turbulence-closure models are available in TELEMAC-3D, see [17] among others. In this study, a constant eddy viscosity model was used.

In all our simulations using the proposed multi-layered finite volume model, the total water height H is assumed to be given and the water heights h_α at the layers are defined using equal fractions as

$$h_\alpha = l_\alpha H \qquad \text{with } l_\alpha = \frac{1}{M},\ \alpha = 1, \ldots, M.$$

Furthermore, the fixed Courant number $Cr = 0.7$ is used and the time step Δt is varied according to the condition (14). The following test examples are selected:

4.1. Lake at rest flow

In this example we solve the benchmark problem of a lake at rest flow proposed in [9] to test the conservation property of numerical methods for single-layer shallow water equations. The lake bed is irregular, so this test example is a good illustration of the significance of the source term treatment for practical applications to natural watercourses. In the current work we consider its multi-layer version. It is expected that the total water free-surface remains constant and the water velocity should be zero at all times. We run the FVC method using a mesh of 100 gridpoints and the obtained results are displayed at time $t = 10\,800$ s as in [9]. In Fig. 3 we present the water interfaces and the water free-surface along with the lake bed. We show the computed results using the single-layer, 5-layer, 10-layer and 20-layer models. For better insight, Fig. 4 presents the errors in the difference between the exact and the computed total water free-surface. As can

[1] Information on the software is available on http://www.opentelemac.org.

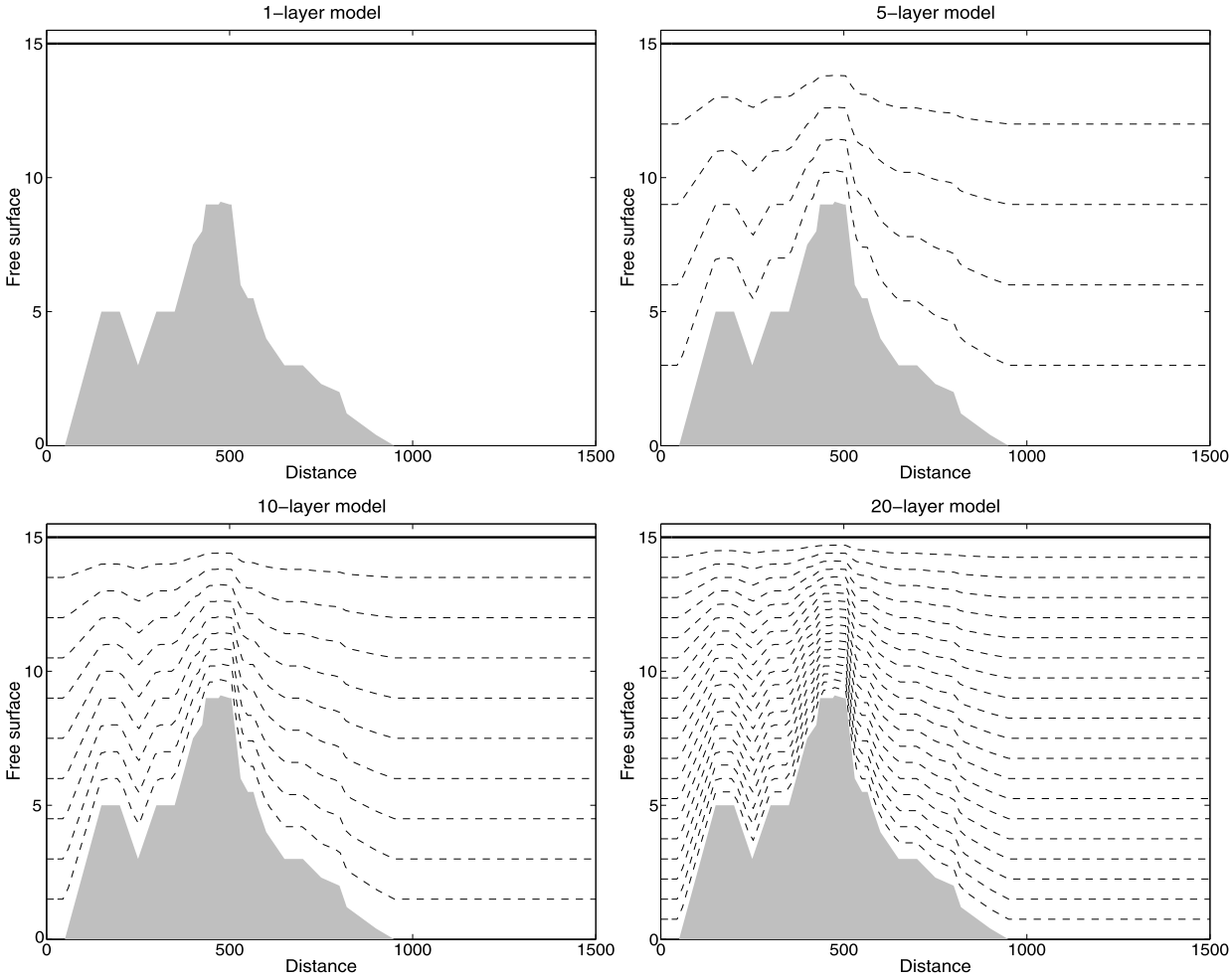


Fig. 3. The water interfaces (dashed lines) and water free-surface (solid line) for the lake at rest flow at time $t = 10800\,s$ using different layers in the multi-layer model.

be seen, the water free-surface remains constant during the simulation times and the proposed FVC method preserves the C-property to the machine precision. It should be stressed that the performance of the FVC method is very attractive since the computed solution remains stable and accurate even when coarse meshes are used without requiring complicated techniques to balance the source terms and flux gradients as those reported in [4,9] among others.

4.2. Dam-break problem on a flat bottom

We consider the dam-break problem in a rectangular channel with flat bottom, *i.e.* $Z(x) = 0$ studied in [3]. The channel is of length 100 and the initial conditions are given by

$$H(0,x) = \begin{cases} 2, & \text{if } x \le 0, \\ 1, & \text{if } x > 0, \end{cases} \qquad u(0,x) = 0.$$

At $t = 0$ the dam collapses and the flow problem consists of a shock wave traveling downstream and a rarefaction wave traveling upstream. The purpose of this test example is to compare the results obtained using our FVC scheme to those computed using the kinetic scheme in [7]. We also use this test example to validate the FVC results to those obtained using the three-dimensional Navier–Stokes equations with free-surface conditions reported in [15]. Following the work in [7], the dimensionless viscosity coefficient $\nu = 0.01$, the gravity $g = 2$, the friction coefficient $\kappa = 0.1$ and the results are presented at time $t = 14$. In Fig. 5 we display the water free-surface obtained using the FVC and kinetic schemes on two different meshes with 50 and 200 gridpoints for the 10-layer model. In this figure we also include a reference solution obtained using the FVC scheme on a fine mesh of 8000 gridpoints. It is clear that at the coarse mesh of 50 gridpoints the solution computed by the kinetic scheme is more diffusive than the FVC solution. This numerical diffusion is substantially reduced by refining the mesh to 200 gridpoints but still the FVC scheme illustrates better results. Similar features have been observed

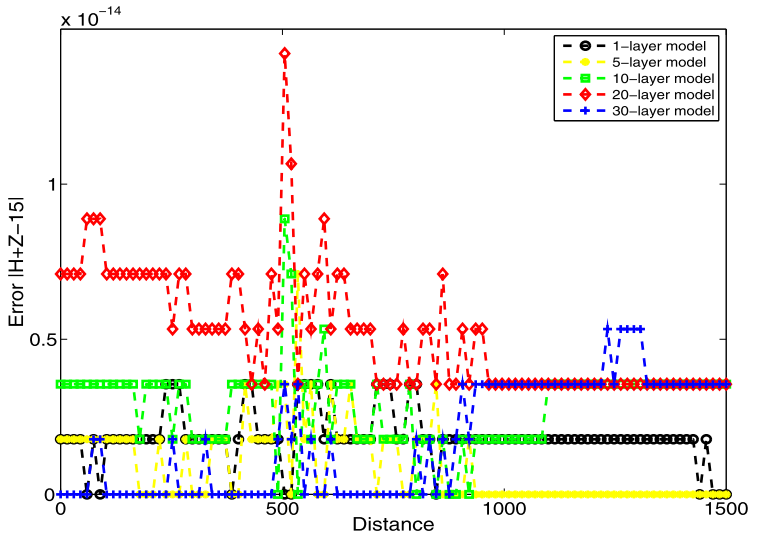


Fig. 4. Errors in the difference between the exact and the computed total water free-surface for the lake at rest flow at time $t = 10\,800$ s.

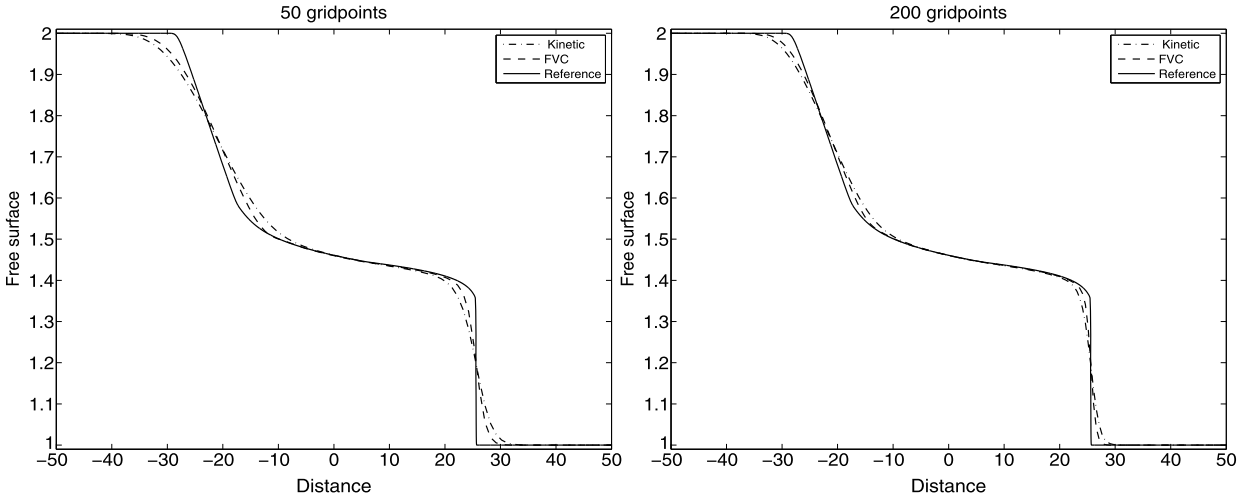


Fig. 5. Water free-surface obtained for the 10-layer model using 50 gridpoints (left) and 200 gridpoints (right) for the dam-break on a flat bottom at $t = 14$.

for a comparison, not reported here, using 20-layer and 50-layer models. The FVC scheme captures correctly the rarefaction and the shock without need for very fine mesh.

The water velocity at the interfaces along with the mean velocity are depicted in Fig. 6 using both selected meshes. It is clear from the velocity plots in this figure that a numerical dissipation is more pronounced in the results obtained using the kinetic schemes than those velocity plots computed using the FVC scheme. Note that the performance of our FVC method is very attractive since the computed solutions remain stable and highly accurate without solving Riemann problems or linear systems of algebraic equations in the hyperbolic parts. The associated 3D simulations for this test example using the TELEMAC-3D are depicted in Fig. 7. Here a mesh of 9840 elements and 5907 nodes is used in the simulation along with a fixed time step $\Delta t = 0.01$ s. Qualitatively, the speed and the location of the moving water front in the 3D results agree well to those simulated by the multi-layered model. It is clear that the 3D results exhibit some fluctuations on the water free-surface which are absent in the results obtained using the multi-layered model. These fluctuations are attributed to the turbulent effects accounted for in the 3D model and are in good agreement with the experimental data report in [21] for dam-break flows.

To further quantify the results for this test example we compare in Fig. 8 the velocity profiles at the location $x = 8$ obtained using the multi-layered shallow water equations to those obtained using TELEMAC-3D and the three-dimensional Navier–Stokes equations at time $t = 14$. We have included results obtained for the 5-layer, 10-layer, 20-layer and 50-layer models using the mesh with 200 gridpoints. Increasing the number of layers in our model results in a better convergence to the velocity profile obtained using the Navier–Stokes equations. Again, compared to the results obtained using the Navier–Stokes equations, the velocity profiles computed using the FVC scheme are more accurate than the results computed using

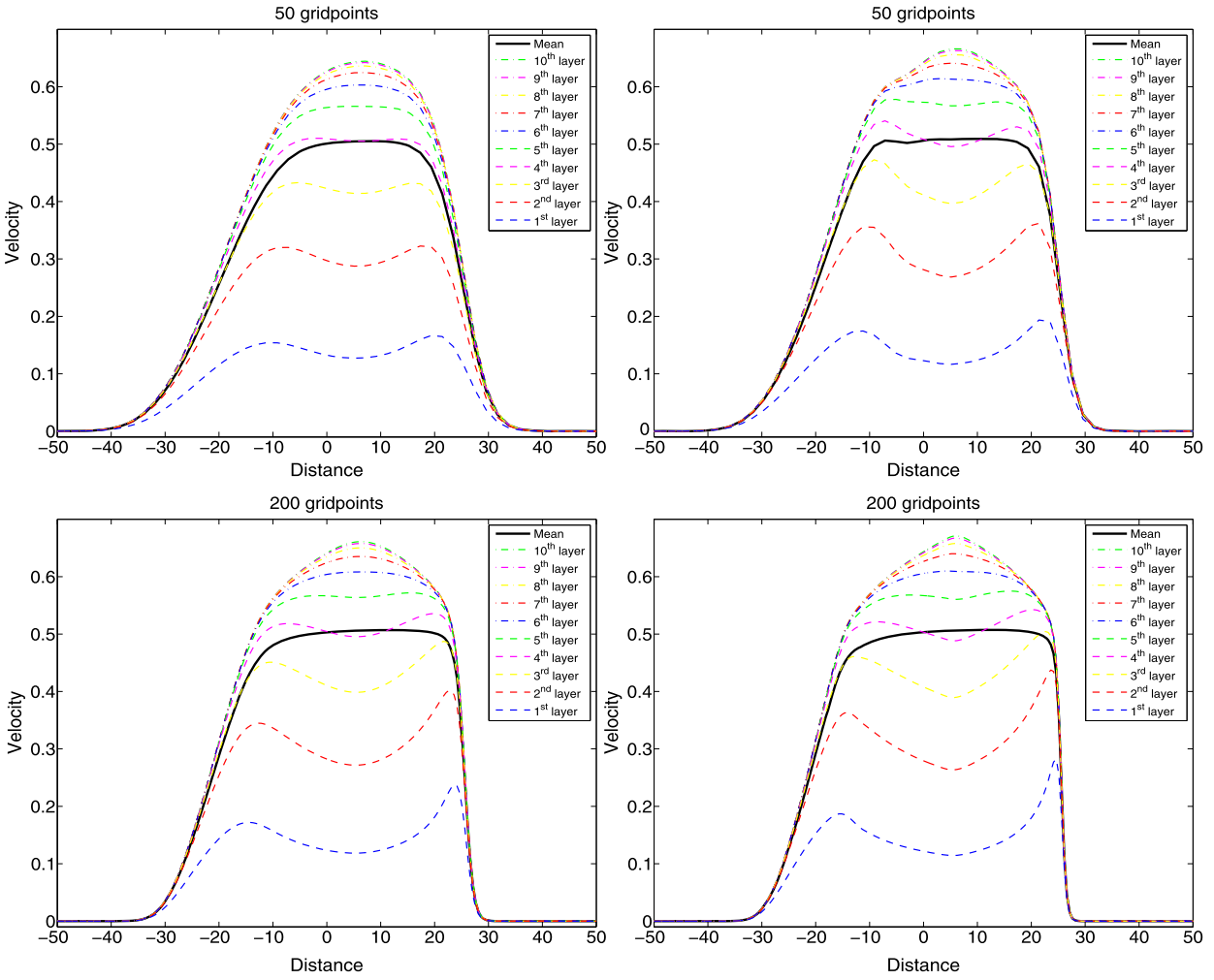


Fig. 6. Water velocity at the interfaces (dashed lines) and the mean velocity (solid line) obtained for the 10-layer model using the kinetic scheme (left) and the FVC scheme (right) for the dam-break on a flat bottom at $t = 14$.

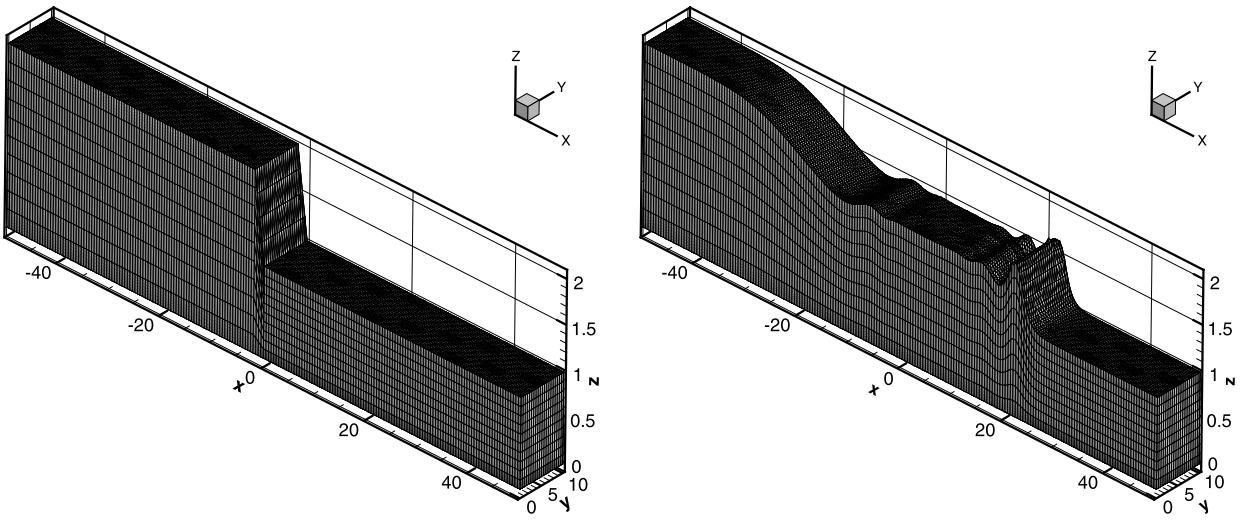


Fig. 7. Initial water free-surface (left) and water free-surface at time $t = 14$ s (right) obtained for the 3D simulation of dam-break problem.

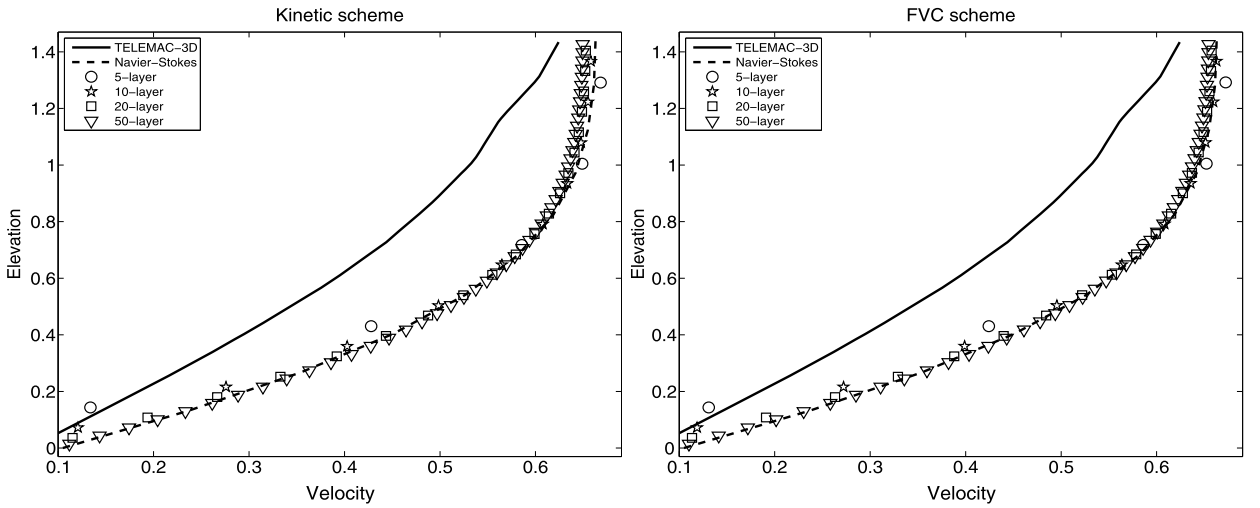


Fig. 8. Velocity profiles at the location $x = 8$ obtained using the kinetic scheme (left) and FVC scheme (right) for the dam-break on a flat bottom at $t = 14$.

Table 1
CPU times (in seconds) for 10-layer and 20-layer models on different meshes for the dam-break on a flat bottom at $t = 14$.

Gridpoints	10-layer model		20-layer model	
	Kinetic scheme	FVC scheme	Kinetic scheme	FVC scheme
200	3.2	3.0	5.4	4.8
400	12.5	9.7	20.8	15.5
800	49.1	34.9	81.9	55.4

the kinetic scheme. Obviously for a given location in the computational domain the water velocity vertically varies within the elevation which is not the case in the conventional single-layer shallow water equations widely used in the literature to model dam-break problems. This test example demonstrates that it is possible to capture the vertical variation in the water velocity using a series of one-dimensional shallow water equations without relying on the three-dimensional Navier–Stokes equations with moving boundary conditions. This results in a significant reduction of computational costs. For the considered dam-break conditions, the FVC scheme produces numerical results as accurate as those computed using the Navier–Stokes equations but with a very low computational cost. Needless to mention the discrepancy between the velocity profiles obtained using the TELEMAC-3D and the FVC methods in Fig. 8. This discrepancy is mainly due to the turbulent effects present in the model for dam-break problems.

In order to highlight the performance of the FVC scheme for this test example we summarize in Table 1 the CPU times for the FVC and the kinetic schemes using meshes with different number of gridpoints. A simple inspection of this table reveals that, for meshes with low number of gridpoints, the measured CPU times are comparable for both schemes. However, for meshes with large number of gridpoints the FVC method is the most efficient. Note that in general, kinetic schemes are based on the set of equations governing the motion of water flows at the continuum level, *i.e.* shallow water equations, can be obtained by taking the moments of the well-known Boltzmann equation at the molecular level with respect to the collision invariants. For water in the state of collisional equilibrium, the collision integral vanishes, and the Boltzmann equation adopts a form similar to that of the linear wave equation. Its solution is simply the Maxwellian probability density distribution function. When moments of this equation are taken with the collision invariants, the shallow water equations are obtained, see for instance [7,22]. For the present test problem, it has been shown that the FVC scheme might be a better compromise between accuracy, stability and efficiency. It should be stressed that the CPU time for the TELEMAC-3D in this test example is about 320 s.

4.3. Wind-driven circulation flow

Our final test example is a class of wind-driven circulation flows proposed in [27]. This type of test examples has widely served as a prototype to verify the performance of multi-layer shallow water flows, see for example [7,29]. In our simulations we use the same flow parameters as in [7]. Hence, the multi-layered equations (9) are solved in a flow domain 16 m long filled at 2 m water under a wind force blowing from the right side of the domain with a speed of $w = 20$ m/s. The viscosity coefficient $\nu = 0.1$ m^2/s, the friction coefficient $\kappa = 0.00001$ m/s, the wind stress coefficient $\gamma_s^2 = 0.0015$, the water density $\rho = 1000$ kg/m^3, the air density $\rho_a = 1.2$ kg/m^3 and the gravity $g = 9.81$ m/s^2. In Fig. 9 we present the velocity fields obtained for 10-layer, 20-layer and 50-layer models using the kinetic and FVC schemes on a mesh of 16 gridpoints at time

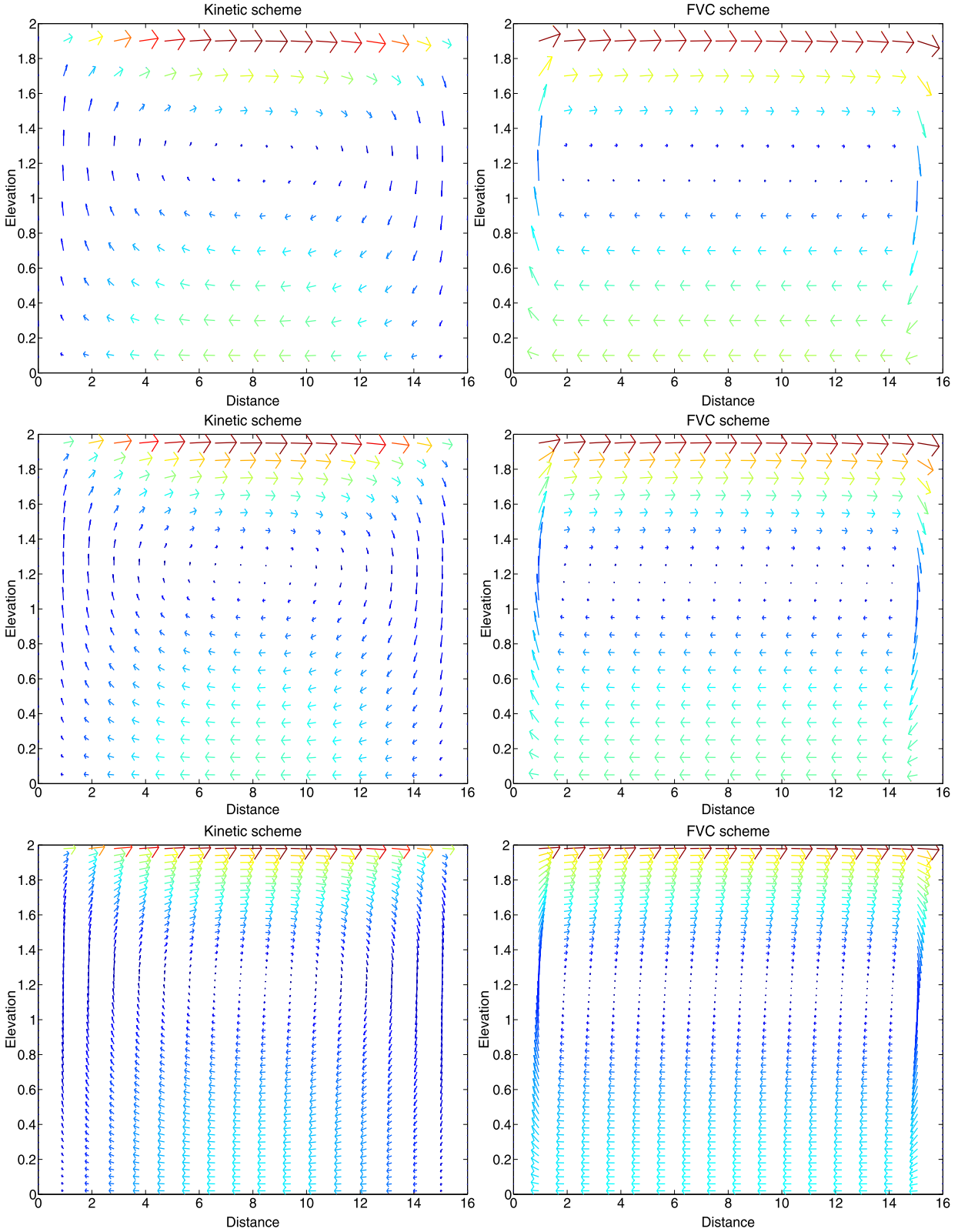


Fig. 9. Velocity fields obtained for 10-layer model (first row), 20-layer model (second row) and 50-layer model (third row) using the kinetic scheme (left column) and FVC (right column) scheme on a mesh of 16 gridpoints at time $t = 20$ s.

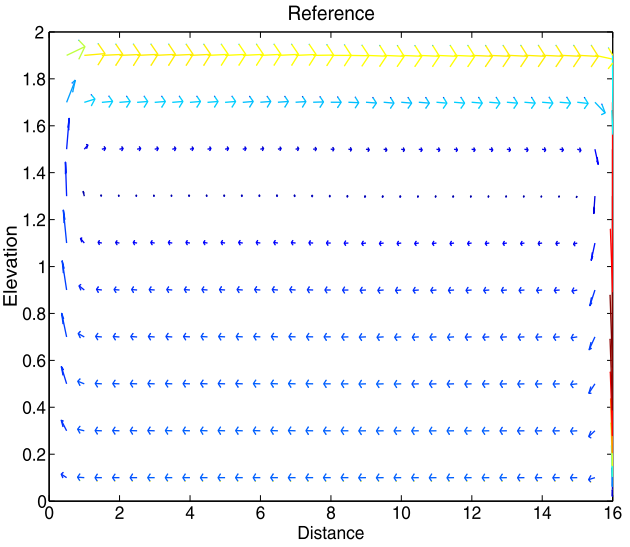


Fig. 10. Reference velocity fields obtained for 10-layer model using the kinetic scheme on a fine mesh of 16 000 gridpoints at time $t = 20$ s.

$t = 20$ s. It is worth remarking that these two-dimensional velocity fields are generated from our one-dimensional results using a post-processing procedure from [7]. Here, the vertical velocity v is recovered from the divergence-free condition

$$\frac{\partial u}{\partial x} + \frac{\partial v}{\partial z} = 0. \tag{39}$$

A similar procedure has also been used in [14]. Thus, to obtain the velocity v Eq. (39) is integrated on each layer using a non-penetration condition at the bottom. As can be seen from the results in Fig. 9 a global recirculation has been formed in the channel center and the center of the vortex is clearly affected by the number of layers used in the simulations. It is also clear that the numerical diffusion is more visible in the kinetic results than the FVC results such that for this test example the kinetic scheme fails to accurately resolve the wall effects on the velocity fields. To further emphasize this point we present in Fig. 10 a reference velocity field obtained for the 10-layer model using the kinetic scheme on a very fine mesh of 16 000 gridpoints. The clear indication from the velocity fields depicted in this figure is that the kinetic scheme requires a very fine mesh to capture the wall effects and produces a high resolution velocity field. On the other hand, we remark that the computed results in Fig. 10 are in good agreement with those simulated using the FVC scheme on the coarse mesh of 16 gridpoints. The obtained results demonstrate the ability of the presented FVC scheme to capture the small flow features within the channel without generating spurious oscillations. For instance, a simple inspection of these results demonstrates that the wall pattern is accurately captured along its transport direction and no noticeable differences are detected between the results obtained using the simulations performed on the coarse mesh of 16 gridpoints and those using the kinetic scheme on the fine mesh of 16 000 gridpoints.

Now, we turn our attention to the performance of the FVC scheme for a test example on wind-driven circulation in a long water channel proposed in [27]. The aim of this test problem is to compare the computed velocity profiles using the FVC scheme to those analytically calculated in [27]. Here, we solve the system (9) in a flat rectangular lake of $3400 \times 1400 \times 10$ m^3 subject to a uniform wind stress of $\sigma = 1.5$ N/m^2 applied at the surface, equivalent to a wind speed of $w = 28.83$ m/s blowing from the left of the lake. As in [27], the viscosity coefficient $\nu = 100$ cm^2/s, the friction coefficient $\kappa = 0.1$ cm/s, the wind stress coefficient $\gamma_s^2 = 0.0015$, the water density $\rho = 1025$ kg/m^3, the air density $\rho_a = 1.2$ kg/m^3 and the gravity $g = 9.81$ m/s^2. It has been shown in [27] that at a given elevation $z \in [-10, 0]$ an analytical solution of the velocity can be derived as

$$u(z) = \beta\left(\frac{z^2}{2\nu} - \frac{H}{\kappa} - \frac{H^2}{2\nu}\right) + \frac{\sigma}{\rho}\left(\frac{z}{\nu} + \frac{1}{\kappa} + \frac{H}{\nu}\right), \tag{40}$$

where

$$\beta = \frac{\frac{\sigma}{\rho}\left(\frac{H^2}{2\nu} + \frac{H}{\kappa}\right)}{\left(\frac{H^3}{3\nu} + \frac{H^2}{\kappa}\right)}.$$

In the first run for this test example we consider the situation of wind-driven circulation flow without bottom friction. For the second run we solve the wind-driven circulation flow with no slip condition. In this case the analytical solution (40) reduces to

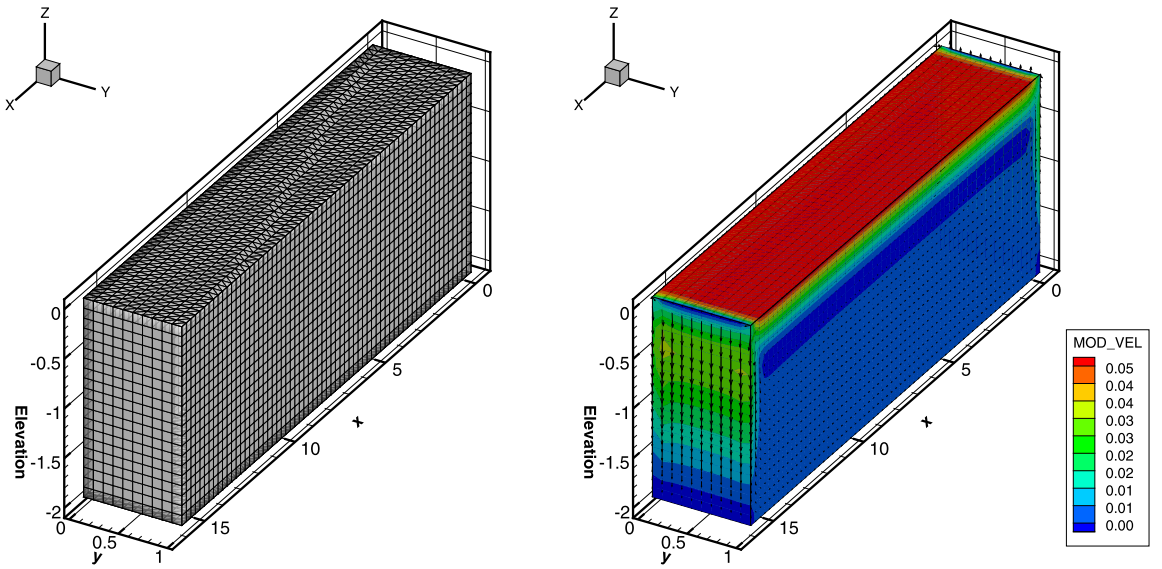


Fig. 11. Initial mesh (left) and velocity field at time $t = 20$ s (right) obtained for the 3D simulation the wind-driven circulation flow.

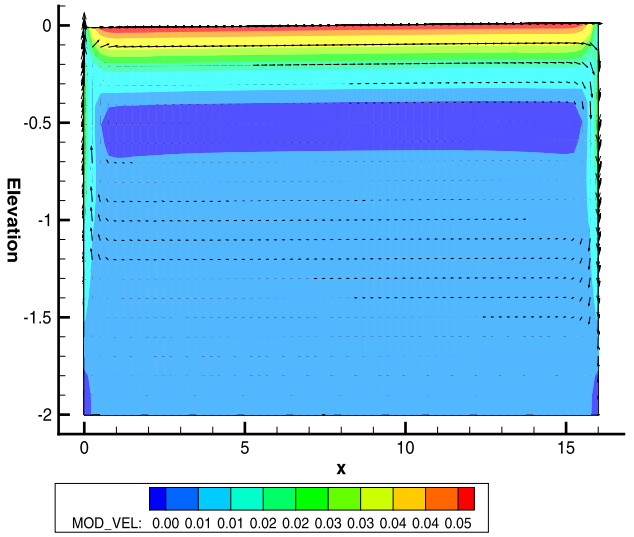


Fig. 12. Projection in the xz plane of the 3D velocity field from Fig. 11.

$$u(z) = \frac{\sigma}{\rho \nu H}\left(\frac{3}{4}z^2 + Hz + \frac{1}{4}H^2\right).$$

It is easy to verify that this velocity profile presents a parabola with two zeros attained at $z = -H$ and $z = -\frac{H}{3}$. The minimum and maximum vertical velocities are $\frac{-1}{12}\frac{\sigma H}{\rho \nu}$ and $\frac{1}{4}\frac{\sigma H}{\rho \nu}$, respectively. The TELEMAC-3D model is also used to solve this test example on a mesh of 25 600 elements and 15 015 nodes shown in the left plot of Fig. 11 using a fixed time step $\Delta t = 1$ s. The obtained velocity field at time $t = 20$ s is presented in the right plot of Fig. 11. Fig. 12 illustrates a cross section of the velocity field in the xz plane. This velocity field shows similar flow features with those detected in the results obtained using the FVC scheme presented in Fig. 9.

Fig. 13 exhibits the velocity profile at the center of the lake, $x = 1700$ m for the wind-driven circulation flow without bottom friction using two meshes of 17 and 170 gridpoints. Those results obtained for the wind-driven circulation flow with no slip condition are presented in Fig. 14. For comparison reasons we have also included in these figures the results obtained using the kinetic scheme. For comparison reason, the velocity profiles for the TELEMAC-3D are also included in Fig. 14. Under actual wind and flow conditions, it is clear that the FVC scheme on both meshes produces the best results compared to the exact solution. It should be stressed that this matching between the analytical and the FVC results is valid only at the center of the lake when the length of the lake is assumed infinitely long. Results on the coarse mesh of

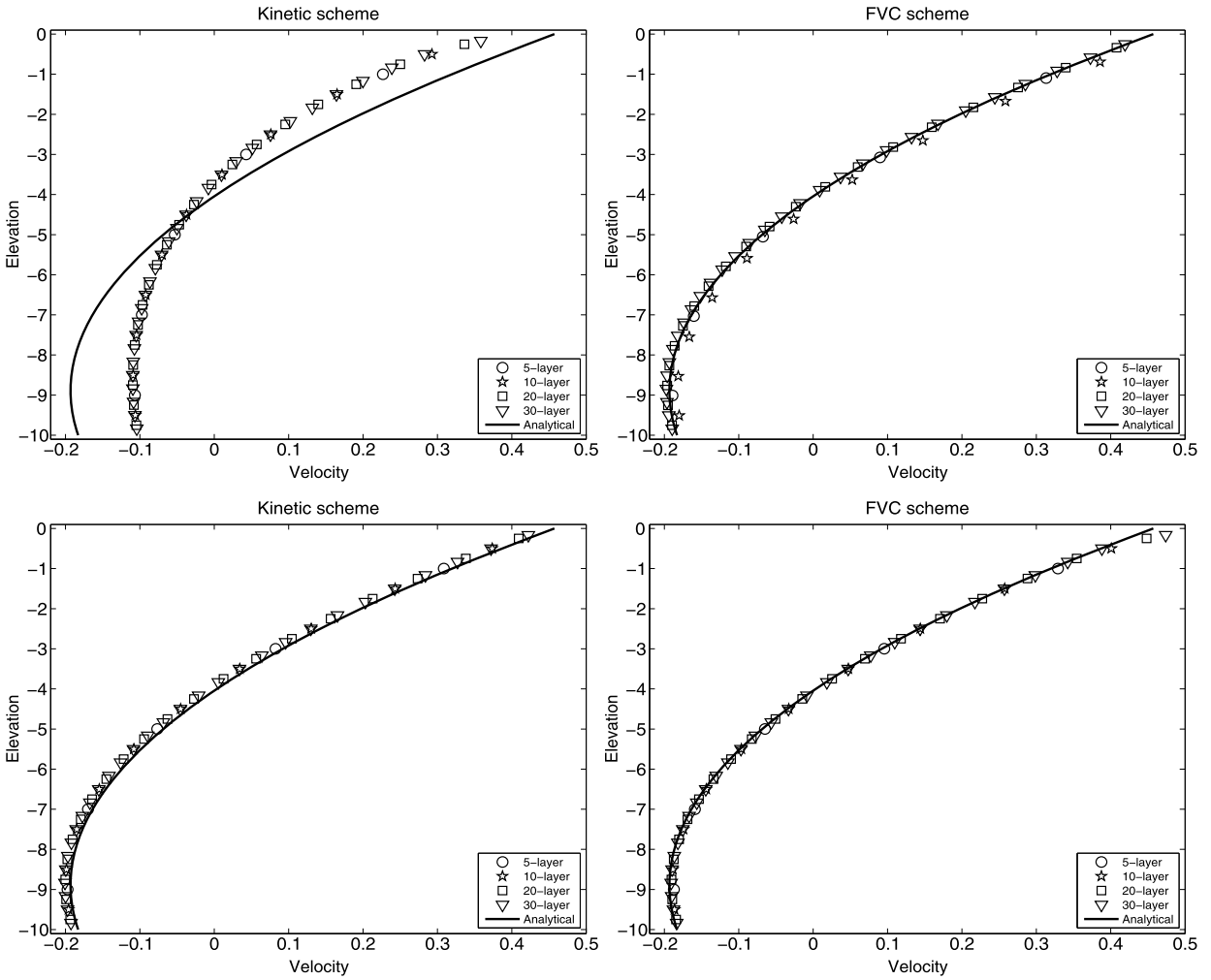


Fig. 13. Comparisons of numerical predictions with the analytical solution for the wind-driven circulation flow without bottom friction using 17 gridpoints (top) and 170 gridpoints (bottom).

17 gridpoints using the kinetic scheme are more dissipative than those obtained using the FVC scheme on the same mesh. It is worth remarking that the velocity profiles obtained for this wind-driven circulation flow on the coarse mesh using the kinetic scheme exhibit a damped behavior near the bed region. This can be explained by the excessive numerical diffusive effect of the kinetic scheme. Overall, the proposed multi-layered finite volume solutions compare well to the analytical solutions. The good agreement between the FVC and the TELEMAC-3D results in Fig. 14 should also be noted. In order to examine the performance of our FVC method over second-order kinetic methods, we have implemented slope limiters in the kinetic solver. The second-order accuracy is achieved in the kinetic scheme by using the MUSCL techniques for the spatial discretization along with the second-order Runge–Kutta method for the time integration. As a slope limiter function we used the well-known van Albada limiter. In Fig. 15 we present the obtained results using the first-order, second-order kinetic schemes and the FVC method for 10-layer and 20-layer models using a mesh of 17 gridpoints. The improvement in accuracy of the second-order kinetic scheme over its first-order counterpart can be clearly seen from the results in Fig. 15. However, for both models with 10 and 20 layers the results obtained using the FVC method are more accurate than those obtained using the second-order kinetic scheme. Compare the numerical diffusion in the results obtained for the lower layers using the second-order kinetic scheme to those obtained using the FVC method in Fig. 15. In terms of efficiency, for all considered numbers of layers the FVC method is the most efficient. For instance, solving the 20-layer model, the FVC method is about 3 times faster than the second-order kinetic scheme.

Our final concern is to check the influence of the mass exchange terms on the multi-layer shallow water results. To this end we perform numerical simulations with exchange term G given by (4) and without exchange term (*i.e.* $G = 0$) and using different values of the eddy viscosity ν in (6). Fig. 16 exhibits the obtained velocity fields for 10-layer model using $\nu = 0$, $\nu = 0.001$ and $\nu = 0.03$. It is evident from the presented results that multi-layer model with mass exchange leads to a recirculation process. Notice that, in this stationary solution, the global discharge for the whole flow is equal to zero but the

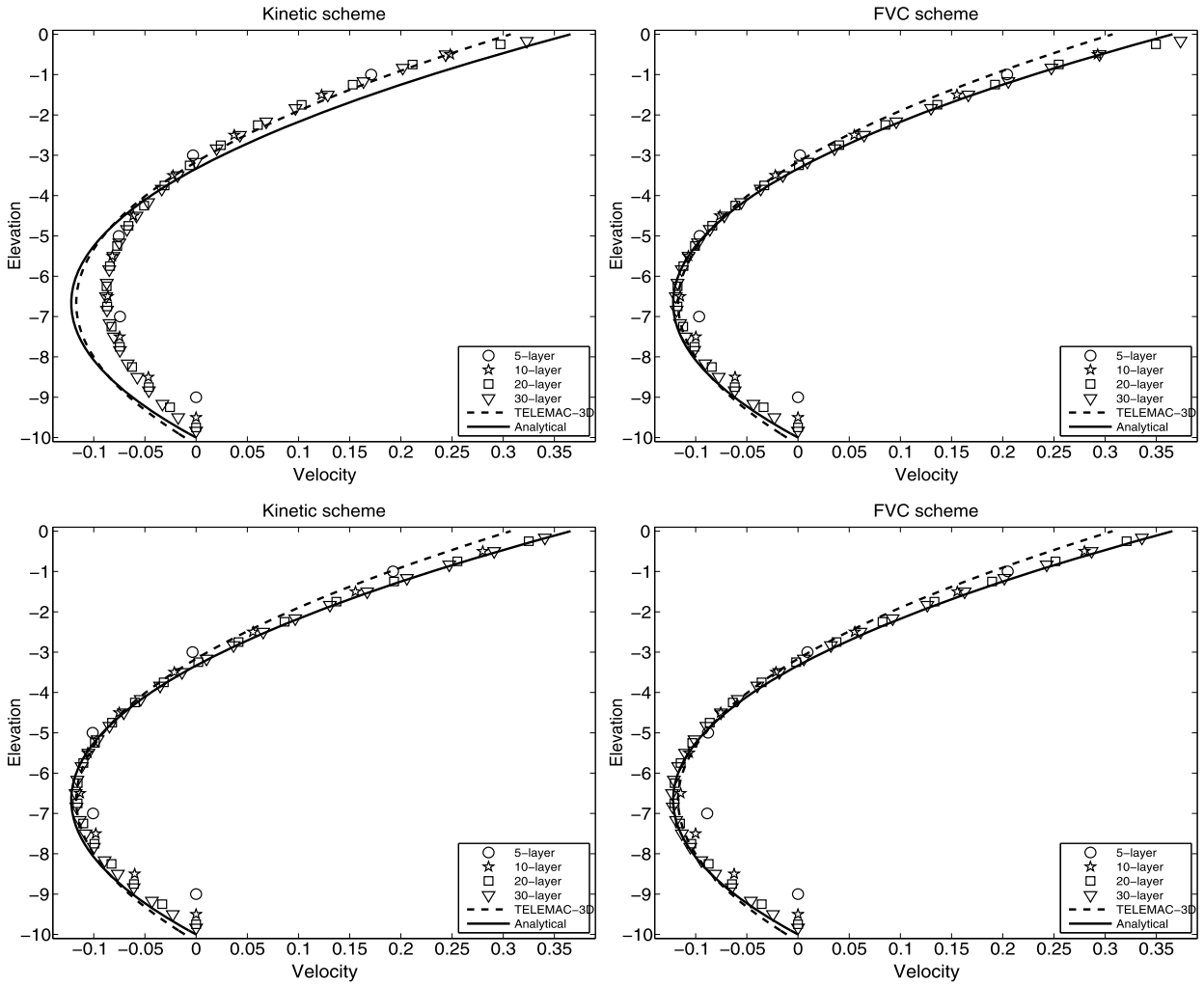


Fig. 14. Comparisons of numerical predictions with the analytical solution for the wind-driven circulation flow with no slip condition using 17 gridpoints (top) and 170 gridpoints (bottom).

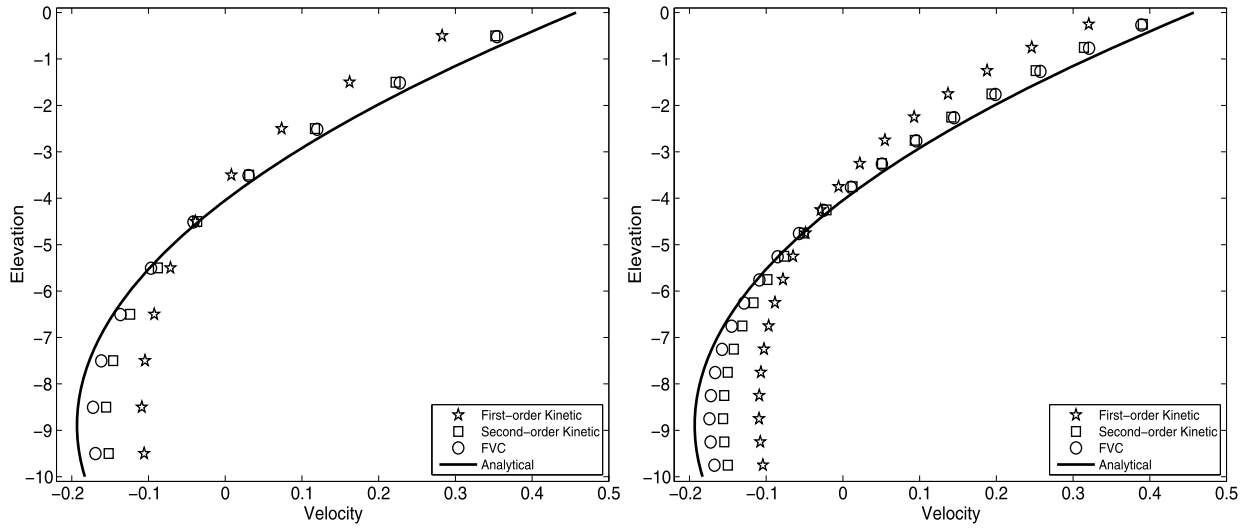


Fig. 15. Velocity fields obtained using first-order kinetic, second-order kinetic and FVC methods for 10-layer model (left plot) and 20-layer model (right plot) using a mesh of 17 gridpoints.

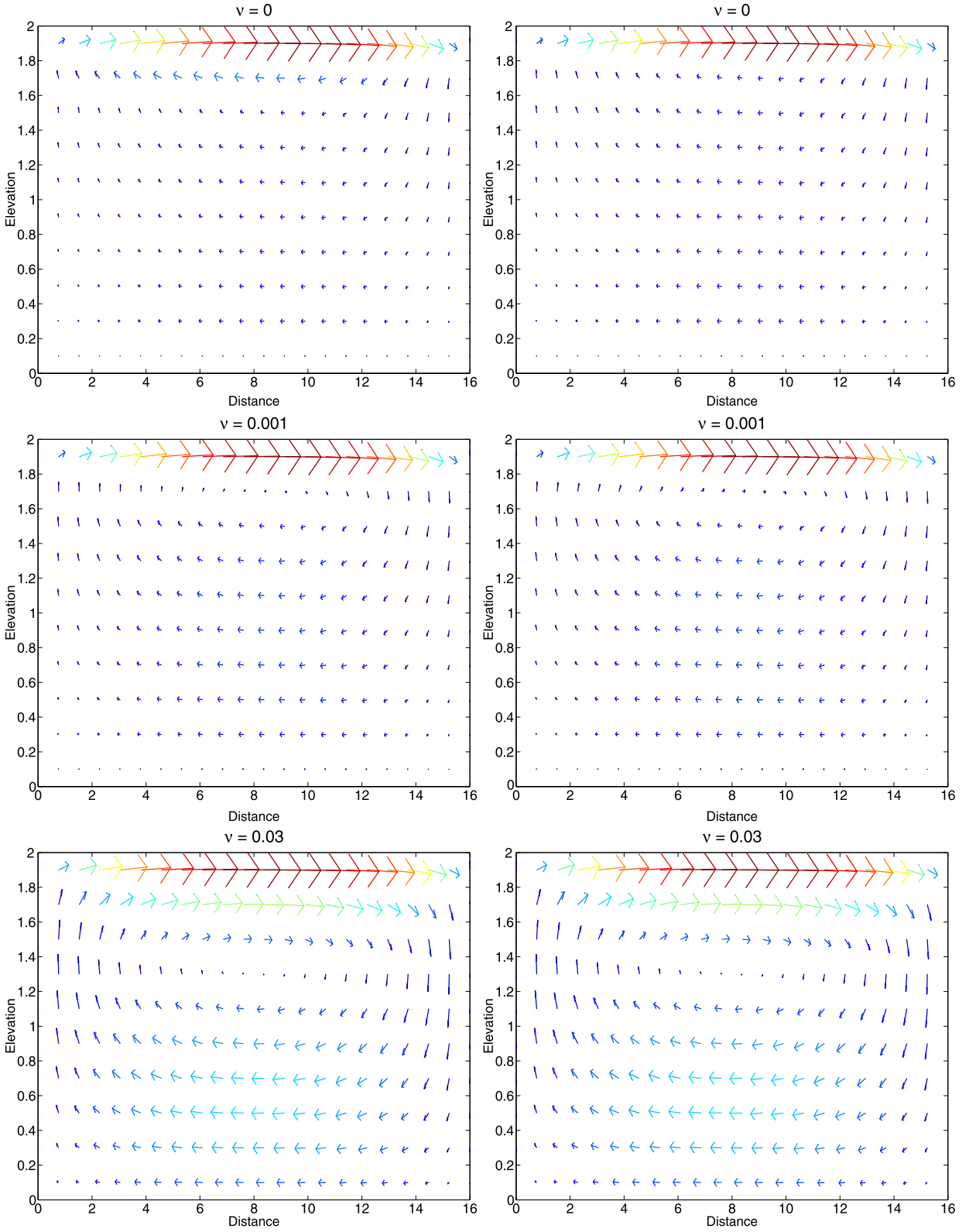


Fig. 16. Velocity fields obtained for 10-layer model with exchange (left column) and without exchange (right column) using a mesh of 16 gridpoints at time $t = 100$ s.

local discharge for each layer is not prescribed a priori. On the other hand, the multi-layer model without mass exchange leads to a lake at rest situation which is very similar to the one obtained by considering a single-layer model. It is worth remarking that, since we consider in this case one mass equation for each layer, a stationary solution has to satisfy the fact that the discharge is constant for each layer. Indeed, since the water discharge is equal to zero at the wall boundaries, it has to vanish everywhere in the computational domain and as a consequence we obtain a lake at rest solution.

It should be stressed that, compared to the classical bi-fluid model without exchange, there are two places where the exchange takes place in the considered multi-layer model: (i) the first one is the term G in the momentum equation and (ii) the second one comes from the fact that we consider only one global mass equation for the whole flow model and not one mass equation per layer. These two modeling facts are linked and cannot be separated such that there is no meaning to consider the current multi-layer model with $G = 0$ since, in its derivation from Navier–Stokes equations, the term G appears naturally in the momentum equation. The main aim of the present study is to consider only one global mass equation for the whole flow model. Therefore, the appearance of the term G in the momentum equation is just a natural consequence of the first choice (i).

5. Conclusions

In this paper we have proposed a new multi-layered finite volume model for shallow water flows with mass exchange. Coupling terms between the layers have been incorporated in the finite volume model. The numerical method combines the attractive attributes of the finite volume discretization and the method of characteristics to yield a robust algorithm for multi-layered shallow water flows with mass exchange. The new method can compute the numerical fluxes corresponding to the real state of water flow without relying on Riemann problem solvers. Furthermore, the proposed approach does not require either nonlinear solution or special front tracking techniques. The method is simple, accurate, easy to implement, and can be used to solve both steady and unsteady shallow water problems. Numerical results and applications have been illustrated for several test problems for multi-layered shallow water flows on flat and non-flat bottom. The presented results demonstrate the accuracy of the new finite volume method and its capability to simulate multi-layered shallow water flows in the hydraulic regimes considered. For the selected test examples, the results obtained using the proposed finite volume method have been compared to those obtained using the kinetic method widely used for multi-layer shallow water flows.

Future work will involve inclusion of viscous coupling a wave model component into the modeling system to include the effects of bottom friction, wind stresses, eddy viscosity, and Coriolis forces in a two-dimensional version of the proposed multi-layered hydrodynamic model. Numerically, the present scheme is a suite of simple finite volume methods that are currently being developed. Other method components will include application to morphodynamic modeling and large-eddy simulation of multi-layered shallow water flows. In many situations, these models will be solved on complex domains and over irregular bathymetries such as coastal scenarios. The proposed finite volume method is particularly advantageous for these types of applications.

Acknowledgements

The work of M. Seaid was supported in part by Centre National de la Recherche Scientifique (CNRS) under the contract # 209821. The authors would like to thank an anonymous referee for giving very helpful comments and suggestions that have greatly improved this paper.

References

[1] R. Abgrall, S. Karni, Two-layer shallow water systems: a relaxation approach, SIAM J. Sci. Comput. 31 (2009) 1603–1627.
[2] F. Alcrudo, F. Benkhaldoun, Exact solutions to the Riemann problem of the shallow water equations with a bottom step, Comput. Fluids 30 (2001) 643–671.
[3] E. Audusse, A multilayer Saint-Venant system: derivation and numerical validation, Discrete Contin. Dyn. Syst., Ser. B 5 (2005) 189–214.
[4] E. Audusse, F. Bouchut, M.O. Bristeau, R. Klein, B. Perthame, A fast and stable well-balanced scheme with hydrostatic reconstruction for shallow water flows, SIAM J. Sci. Comput. 25 (2004) 2050–2065.
[5] E. Audusse, M.O. Bristeau, A well-balanced positivity preserving second-order scheme for shallow water flows on unstructured grids, J. Comput. Phys. 206 (2005) 311–333.
[6] E. Audusse, M.O. Bristeau, M. Pelanti, J. Sainte-Marie, Approximation of the hydrostatic Navier–Stokes system for density stratified flows by a multilayer model: kinetic interpretation and numerical solution, J. Comput. Phys. 230 (2011) 3453–3478.
[7] E. Audusse, M.O. Bristeau, B. Perthame, J. Sainte-Marie, A multilayer Saint-Venant system with mass exchanges for shallow water flows. Derivation and numerical validation, Math. Model. Numer. Anal. 45 (2011) 169–200.
[8] F. Benkhaldoun, M. Seaid, A simple finite volume method for the shallow water equations, J. Comput. Appl. Math. 234 (2010) 58–72.
[9] A. Bermudez, M.E. Vázquez-Cendón, Upwind methods for hyperbolic conservation laws with source terms, Comput. Fluids 23 (1994) 1049–1071.
[10] F. Bouchut, T. Morales, An entropy satisfying scheme for two-layer shallow water equations with uncoupled treatment, Math. Model. Numer. Anal. 42 (2008) 683–698.
[11] F. Bouchut, V. Zeitlin, A robust well-balanced scheme for multi-layer shallow water equations, Discrete Contin. Dyn. Syst., Ser. B 13 (2010) 739–758.
[12] M.J. Castro, J. Macías, C. Parés, A Q-scheme for a class of systems of coupled conservation laws with source term. Application to a two-layer 1D shallow water system, Math. Model. Numer. Anal. 35 (2001) 107–127.
[13] D. Farmer, L. Armi, Maximal two-layer exchange over a sill and through a combination of a sill and contraction with barotropic flow, J. Fluid Mech. 164 (1986) 53–76.

[14] E.D. Fernández-Nieto, E.H. Koné, T. Chacón, A multilayer method for the hydrostatic Navier–Stokes equations: a particular weak solution, J. Sci. Comput. 57 (2013) 1–30.
[15] J.F. Gerbeau, B. Perthame, Derivation of viscous Saint-Venant system for laminar shallow water: numerical validation, Discrete Contin. Dyn. Syst., Ser. B 1 (2001) 89–102.
[16] J. Gula, V. Zeitlin, F. Bouchut, Instabilities of buoyancy-driven coastal currents and their nonlinear evolution in the two-layer rotating shallow water model. Part 2. Active lower layer, J. Fluid Mech. 665 (2010) 209–237.
[17] J.M. Hervouet, Hydrodynamics of Free Surface Flows. Modelling with the Finite Element Method, John Wiley & Sons, Ltd., 2007.
[18] A. Kurganov, G. Petrova, Central-upwind schemes for two-layer shallow water equations, SIAM J. Sci. Comput. 31 (2009) 1742–1773.
[19] J. Lambaerts, G. Lapeyre, V. Zeitlin, Moist versus dry baroclinic instability in a simplified two-layer atmospheric model with condensation and latent heat release, J. Atmos. Sci. 69 (2012) 1405–1426.
[20] J. Lambaerts, G. Lapeyre, V. Zeitlin, F. Bouchut, Simplified two-layer models of precipitating atmosphere and their properties, Phys. Fluids 23 (2011) 046603.
[21] H. Ozmen-Cagatay, S. Kocaman, Dam-break flows during initial stage using SWE and RANS approaches, J. Hydraul. Res. 48 (2010) 603–611.
[22] B. Perthame, C. Simeoni, A kinetic scheme for the Saint-Venant system with a source term, Calcolo 38 (2001) 201–231.
[23] J. Pudykiewicz, A. Staniforth, Some properties and comparative performance of the semi-lagrangian method of Robert in the solution of advection-diffusion equation, Atmos.-Ocean 22 (1984) 283–308.
[24] A. Robert, A stable numerical integration scheme for the primitive meteorological equations, Atmos.-Ocean 19 (1981) 35–46.
[25] P.L. Roe, Approximate Riemann solvers, parameter vectors and difference schemes, J. Comput. Phys. 43 (1981) 357–372.
[26] M. Seaid, On the quasi-monotone modified method of characteristics for transport–diffusion problems with reactive sources, Comput. Methods Appl. Math. 2 (2002) 186–210.
[27] N.J. Shankar, H.F. Cheon, S. Sankaranarayanan, Multilevel finite-difference model for three-dimensional hydrodynamic circulation, Ocean Eng. 24 (1997) 785–816.
[28] C. Temperton, A. Staniforth, An efficient two-time-level semi-lagrangian semi-implicit integration scheme, Q. J. R. Meteorol. Soc. 113 (1987) 1025–1039.
[29] K.R. Tubbs, F.T.C. Tsai, Multilayer shallow water flow using lattice Boltzmann method with high performance computing, Adv. Water Resour. 32 (2009) 1767–1776.
[30] C. Vreugdenhil, Two-layer shallow-water flow in two dimensions, a numerical study, J. Comput. Phys. 33 (1979) 169–184.
[31] V. Zeitlin, Nonlinear Dynamics of Rotating Shallow Water: Methods and Advances, Elsevier, 2007.